Fall 2015

An Evaluation of the Disposition of R941000, a Tetrazolone-Telmisartan Analog: A Case Study of the Suitability of Tetrazolone As a Carboxylic Acid Bioisostere

Ryan Brant Murray
San Jose State University

AN EVALUATION OF THE DISPOSITION OF R941000, A TETRAZOLONE-TELMISARTAN ANALOG IN RATS: A CASE STUDY ON THE SUITABILITY OF TETRAZOLONE AS A CARBOXYLIC ACID BIOISOSTERE

A Thesis

Presented to

The Faculty of the Department of Chemistry

San José State University

In Partial Fulfilment

of the Requirements for the Degree

Master of Science

By

Ryan Murray

December 2015

The Designated Thesis Committee Approves the Thesis Titled

AN EVALUATION OF THE DISPOSITION OF R941000, A TETRAZOLONE-TELMISARTAN ANALOG IN RATS: A CASE STUDY ON THE SUITABILITY OF TETRAZOLONE AS A CARBOXYLIC ACID BIOISOSTERE

by

Ryan Murray

APPROVED FOR THE DEPARTMENT OF CHEMISTRY

SAN JOSÉ STATE UNIVERSITY

December 2015

Dr. Joseph Pesek	Department of Chemistry
Dr. Roger Terrill	Department of Chemistry
Dr. Christophe Colas	Department of Pharmacokinetics, Rigel Pharmaceuticals

Abstract

Carboxylic acids are ubiquitous in medicinal compounds, such as nonsteroidal anti-inflammatories, statins, hypertensives, and anticoagulants. Despite their prolific use, unfavorable characteristics such as metabolic instability, poor membrane permeability, and toxicity have been associated with this moiety in some instances. Bioisosteres have been employed to attenuate these issues. However, bioisostere use can alter drug potency and disposition. Recently, our company demonstrated the feasibility of the tetrazolone moiety as a carboxylic acid bioisostere for the angiotensin II antagonist telmisartan. R941000 (telmisartan-tetrazolone analog) was a potent *in vitro* inhibitor of angiotensin II and possessed a similar disposition to telmisartan. To the best of our knowledge, no studies of the changes in disposition caused by bioisosteric replacement of a carboxylic acid with a tetrazolone have been published. In this work, the disposition of R941000 was evaluated in Sprague Dawley rats, and *in vitro* metabolism was conducted using human and rat hepatocytes and supplemented microsomes. Results indicated comparable PK parameters for R941000 relative to telmisartan, respectively, bioavailability (64.7% vs 59.2%), exposure (2610 ngL/h vs 1850 ngL/h) Cl_{pred} (4.51 ml/min vs 7.23 ml/min) t1/2 (5.37h vs 3.64 h) and V_{ss} (1.67L/kg vs 1.59L/kg). Both compounds underwent biliary excretion, and glucuronide metabolites were found in rat bile; however, no significant glucuronidation was observed in *in vitro* assays. Additional studies utilizing tetrazolone bioisosteres in other species and classes of compounds are needed to further characterize their utility as a carboxylic acid substitute.

ACKNOWLEDGEMENTS

I would like to express my gratitude to San Jose State University for allowing me to pursue my research in both academia and the private sector. I would like to thank the department of chemistry for the opportunity to write and present my thesis work. Additionally, I would like to thank Rigel Pharmaceuticals and the DMPK department for their support of me in my graduate studies. To my committee members, Dr. Pesek, Dr. Terrill, and Dr. Colas, I am very grateful for your insight, suggestions, guidance, and time. To my research advisor, Dr. Pesek, thank you very much for your flexibility and helping me find a project I could pursue while working full time.

To my beautiful family Toni and Ruby, thank you for all your support and patience while I have been pursuing my degree. I am very grateful for all the motivation and encouragement both of you have given me during this time.

Table of Contents

List of Figures

List of Tables

1.0 Introduction

Bioisosteres are functional groups consisting of atom(s) that exhibit similar shape, volume, and/or electronic properties, and elicit comparable biological responses as the chemical moieties they replace.[1,2,3,4] Sage use of bioisosteres can be critical for medicinal chemists attempting to optimize the pharmacological properties of a chemical scaffold, including improved ADME (absorption, distribution, metabolism, excretion) properties and safety profile.[1,2] Additionally, bioisosteres can generate additional intellectual property (IP) space.[1]

Carboxylic acid functional groups are important for many biochemical reactions and can be found in endogenous substances such as prostanoids and amino acids. Due to its low pKa, carboxylic acid exists as an ionized species at physiological pH. This unique feature along with its important biological roles (i.e. β-oxidation, elongation of fatty acids and prostaglandin synthesis, etc.) allow for carboxylic acid to play a critical part in the pharmacophores of many drugs. Indeed, carboxylic acid can be found in >450 drugs marketed today.[1] Despite their widespread use in medicinal compounds, carboxylic acids can be subject to liabilities such as metabolic instability, poor membrane permeability, and toxicity, in some cases. A variety of bioisosteres have been employed to attenuate these liabilities and improve function such as tetrazoles, isothiazoles, and hydroxamic acids, to name a few.[1]

While carboxylic acid bioisosteres have been used successfully, use of functional group surrogates remains a subtle art. Replacement of a molecular moiety with an

"equivalent" group may result in a pharmacologically inactive compound or molecule with dramatically altered ADME behavior.[1] It is therefore important to screen bioisosteres for changes in potency and disposition. For these reasons, it is advantageous to have a palette of chemical "similars" to work with when optimizing compounds.

Recently, our company demonstrated a facile one pot synthesis of tetrazolones and postulated their potential suitability as a carboxylic acid substitute due to similarity in structure with tetrazoles. Additionally, the tetrazolone moiety possesses an acidic hydrogen with a pKa equivalent to a carboxylic acid and has a planar structure. A telmisartan tetrazolone analog (R941000, see Figure 1) was synthesized and found to have excellent potency relative to telmisartan (IC_{50} = 1.7nM v 5.7nM) respectively, for inhibition of AT_1 receptor.[5] Moreover, R941000 demonstrated comparable ADME behavior in Sprague Dawley (SD) rats.

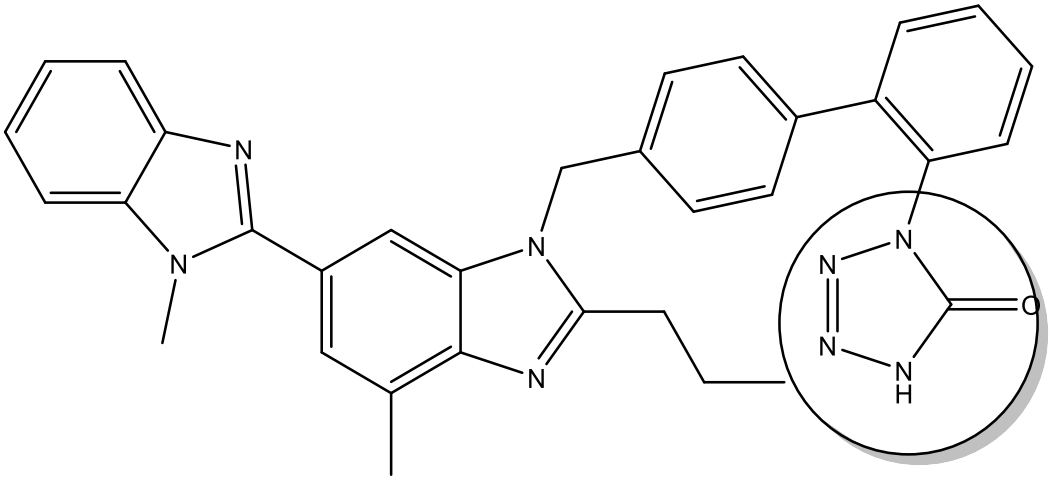

Figure 1. The chemical structure above depicts R941000 with the tetrazolone moiety circled.

Examples of tetrazolone use in medicinal compounds are sparse, and non-existent when assessing changes in drug disposition. Understanding how various moieties affect the ADME characteristics is vital in developing lead compounds that will succeed in a clinical setting. It is the intent of this thesis to evaluate the suitability of tetrazolones, a bioisostere for carboxylic acids in terms of disposition, using R941000 as a model compound, SD rats as a model pre-clinical species, and cryopreserved hepatocytes and microsomes as an *in vitro* platform to predict human disposition.

1.1 Drug Disposition: Principles of ADME

Drug disposition, or ADME, is the study of how a drug behaves once it has been administered.[6,7] When a drug is taken, it gets absorbed, is distributed throughout the body and is eliminated either as the parent drug or metabolite. Understanding drug disposition is critical to proper drug administration, and allows for reasonable estimates of what drug concentration will be over time, permitting establishment of a safe and effective dosing regimen (See Figure 2). As can be seen on the right side in Figure 2, the drug concentration over time is plotted for an orally administered drug. The total exposure, AUC (area under the curve) is shown along with the therapeutic window, between MTC (minimum toxic concentration) and MEC (minimum effective concentration). Factors responsible for drug disposition can be broken down into two interrelated areas of study: pharmacokinetics and drug metabolism. A brief description of each will follow.

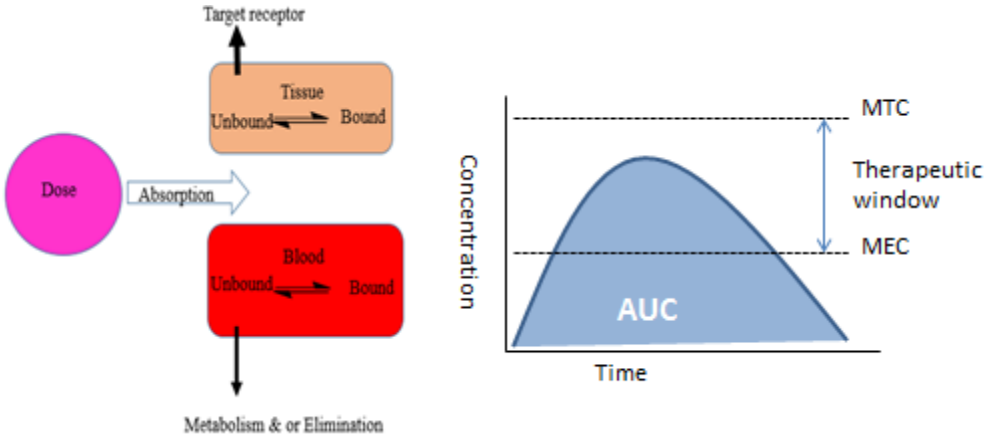

Figure 2. An illustration of the ADME behavior of a drug and therapeutic index are shown above.

1.2 Basic Pharmacokinetic Principles

Pharmacokinetics (PK) is the study of the time course of a drug as it relates to ADME principles.[6] Since drugs are typically eliminated by circulating in blood through organs such as the liver and kidney, taking blood measurements over time can be effective in determining the rate of drug elimination and, consequently, the establishment of safe dosing regimens. Additionally, there is often a relationship between drug concentration in blood and therapeutic effect, making accurate knowledge of a compound's concentration over time critical for effective dosing.

Many mathematical models have been used to explain the PK profiles of drugs, the simplest of which is described by Equation 1 (for an intravenously [IV] administered drug).[6]

$$(1)\ C = \frac{D}{V} e^{\frac{-Cl*t}{V}}, or\ C = Ae^{-kt}$$

Where C is the concentration (in blood or plasma) at any time, D is the dose amount, V is the volume of distribution, Cl is clearance, t is time, and k is the elimination rate constant (Equation 2) and is usually estimated by determining the slope of the terminal phase of a linear graph of concentration over time (see Figure 3). Cl and V are primary pharmacokinetic parameters, which can be used to determine secondary yet important factors like drug half-life (Equation 3) and total drug exposure AUC (Equation 4).[6]

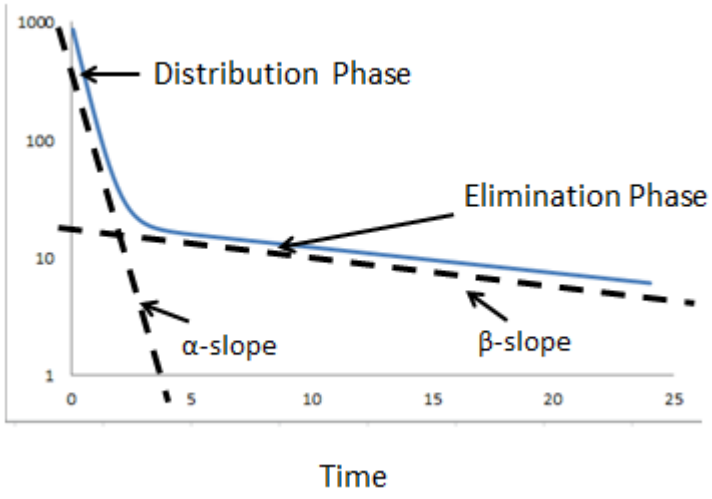

Figure 3. A depiction of the change in drug concentration over time in a linear plot for an IV administered drug is shown above. In the figure both the distributive phase (described by the α slope) and the elimination phase (β slope) can be seen.

(2) $k = \frac{Cl}{V}$

(3) $t_{1/2} = \frac{Ln(2)}{K}$

(4) $AUC = \int_0^t Cdt$

Clearance is one of the most important pharmacokinetic parameters, and describes the rate at which a substance is removed from the blood or plasma.[6] Due to its simplicity and minimal required information, early PK studies often calculate whole body clearance by dividing the IV dose by the total IV exposure, AUC_{IV} (Equation 5). Since IV administered drugs are completely absorbed and AUC is the total resultant exposure from a dose (D), dividing D over AUC (D = mg/kg AUC = ng/ml/kg*h) results in Cl values of ml/h. Cl incorporates the body's ability to enzymatically modify and physically remove a substance. Knowing the Cl of a compound is important in establishing its half-life, and from there a proper dosing regimen.

(5) $Cl = \frac{Div}{AUCiv}$

Volume of distribution (V) is the theoretical volume that would be required for an administered drug that is evenly distributed to match the measured blood plasma concentration.[6,8] There are approximately 5 L of blood and 40 L of intracellular fluid in an adult 70 kg person.[6,8] Compounds with little tissue distribution will remain mostly in the body's central compartment and have a relatively low V, while a drug that highly distributes to other tissues will have a high volume of distribution. V does not represent an actual volume; indeed, some drugs have V values exceeding 500 L, far greater than the actual volume on any individual. These large values are often achieved through several factors such as transporters actively taking up compound into tissues, or nonspecific binding to blood and cellular proteins.[6,8]

While an abstract value, V is important because it affects the systemic concentration of a compound and consequently the concentration of drug a receptor or metabolizing enzyme will see, thus influencing the degree of drug response and the elimination constant, k (see Equations 1-3). Figure 4 shows the volumes of various "compartments" for humans, as well as what constitutes low, medium, and high volume drugs.

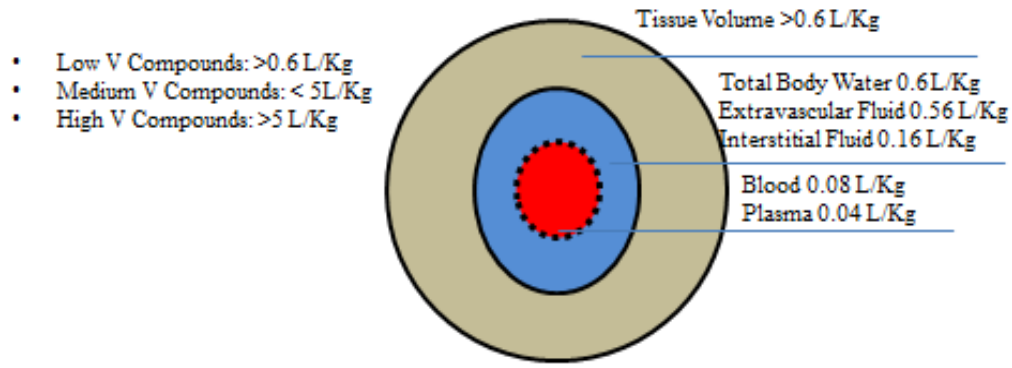

Figure 4. The above figure shows the total fluid volume per Kg for humans. Values for tissue, total body water, blood, and plasma volumes are given along with a definition of low, moderate, or high volume values.[8]

Another important PK parameter to consider is the bioavailability of a drug (%F). An orally administered drug on the other hand may only be partially dissolved, absorbed in the gut with the rest eliminated in the feces, or metabolized before reaching systemic circulation. A common practice in determining the amount of drug absorbed from an oral (PO) dose is to normalize the PO dose to the IV dose and divide the oral exposure by the intravenous exposure (see Equation 6).[6]

$$(6)\ \%F = 100 * \frac{dose_{IV} * AUC_{PO}}{dose_{PO} * AUC_{IV}}$$

1.3 Drug Metabolism

Drug metabolism is the study of how xenobiotic transforming enzymes modify compounds to expedite their elimination from the body.[7,9] These enzymes typically function by adding polarity to the molecules, thereby shifting the decreasing distribution of the molecule to the central compartment where it can more readily be excreted into the urine or feces (See Figure 5).[7] Understanding the mechanisms behind these enzymatic biotransformations is important for developing compounds with favorable dispositions.

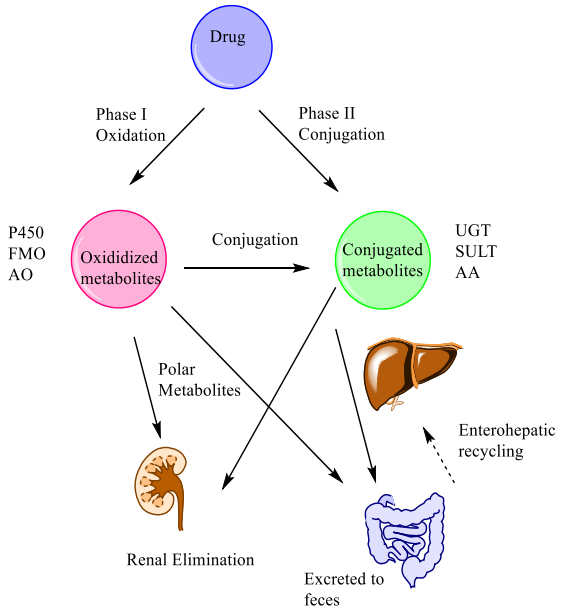

Figure 5. The above illustration details the metabolic fate of a drug through phase I and II metabolism.[7,9]

Drug metabolism is divided into two types: phase I metabolism, involving mainly oxidation reactions, and phase II metabolism, which employs coupling mechanisms to conjugate a xenobiotic to a polar functional group.[7] Important phase I enzymes include cytochrome p450 (P450), flavonoid mono oxygenase (FMO), and aldehyde oxidase

(AO).[9] Uridine glucuronosyltransferase (UGT), and sulfotransferase (SULT) are two of the predominant enzymes responsible for phase II metabolism of drugs. Many of these enzymes are found at high concentrations in the liver and intestine. In this work, P450 and UGT enzymes were the most relevant biotransforming enzymes.

Cytochrome P450 is in a family of heme containing enzymes found on the cytosolic side of the endoplasmic reticulum of a cell. They exist in particularly high concentrations in the liver.[7] P450s are unique in their chemistry since they can utilize molecular oxygen to insert a single oxygen atom into alkyl groups. This can add polarity to a molecule or a potential site for phase II reactions that may help expedite their removal. The overall P450 reaction is shown in Equation 7.

$$(7)\ \mathrm{RH\ (substrate)} + \mathrm{O_2} + \mathrm{NADPH} + \mathrm{H^+} \rightarrow \mathrm{ROH} + \mathrm{H_2O} + \mathrm{NADP^+}$$

A full explanation of the catalytic cycle and mechanisms behind this remarkable enzyme is beyond the scope of this text, but more detailed explanation can be found in references 7, 9. Figure 6, however, illustrates the enzymes, cofactors, and substrates involved in the overall reaction. Electrons are transferred from NADPH through various P450 reductase proteins to the P450 heme complex. From here, iron and oxygen are reduced to a short lived Fe-O_2 state, which is rapidly protonated twice, releasing water, forming the oxidized species, compound I or $O=Fe^{IV\cdot+}$.[7,9] P450s are capable of modifying a wide range of compounds, with substrates typically susceptible to hydrogen abstraction. Common substrates include carbon atoms alpha to hetero atoms such as O, and N, or

alkyl chains, alkenes, and aromatic rings.[9] Additionally, hetero atoms N and S are occasional substrates.[9]

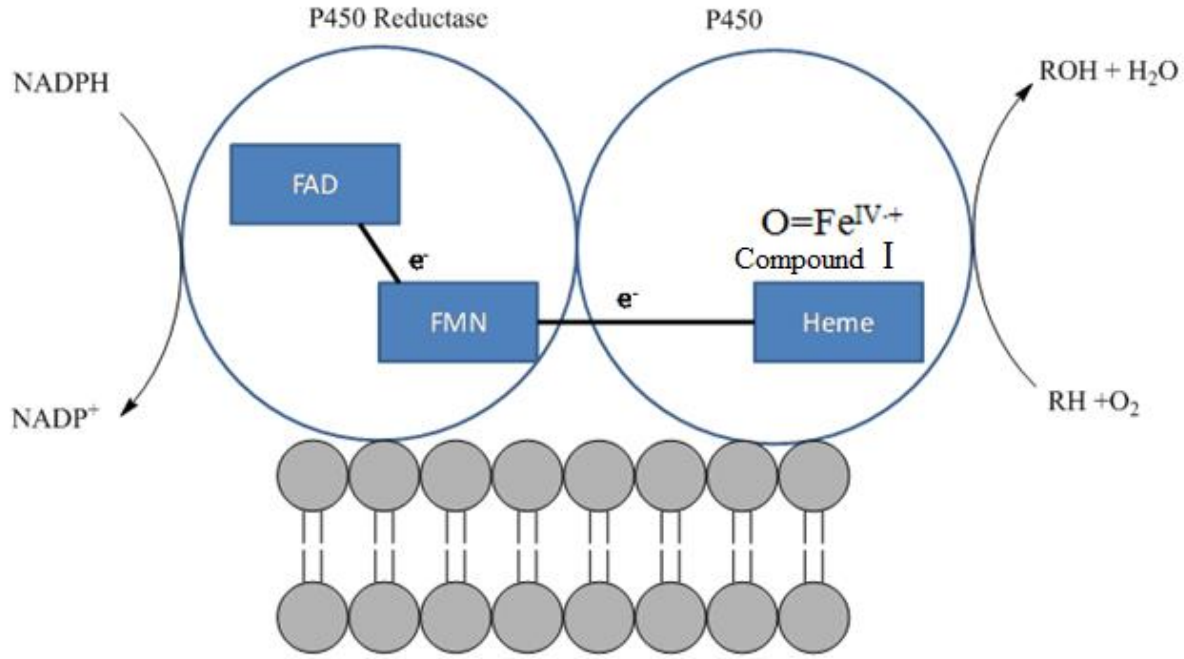

Figure 6. In the diagram above, the electron chain transfer for cytochrome P450 is shown. Electrons are transferred from NADPH, through P450 reductase to the heme group in the P450 protein where a reactive Fe^{IV}oxo intermediate inserts a single oxygen through HAT or SET mechanisms.[7,9]

UGTs consist of four super families: UGT1, UGT2, UGT3, and UGT8. They are found in high concentrations in the liver and gut, but are also expressed in many other tissues such as kidneys, skin, brain, and various glands. Like P450 enzymes they are located on the ER, but on the lumen rather than the cytosolic side.[9]

Candidates for UGT glucuronidation include compounds containing nucleophilic centers such as phenols, alcohols, amines, and carboxylic acids. Figure 7 depicts the catalytic cycle of UGT enzymes. UDPGA is then amenable to nucleophilic attack at the

electrophilic C_1 position of the glucuronide, with UDP as the leaving group. Glucuronide conjugates from UGT result in the formation of polar β-glucuronides that can be excreted in the urine or feces.[7,9]

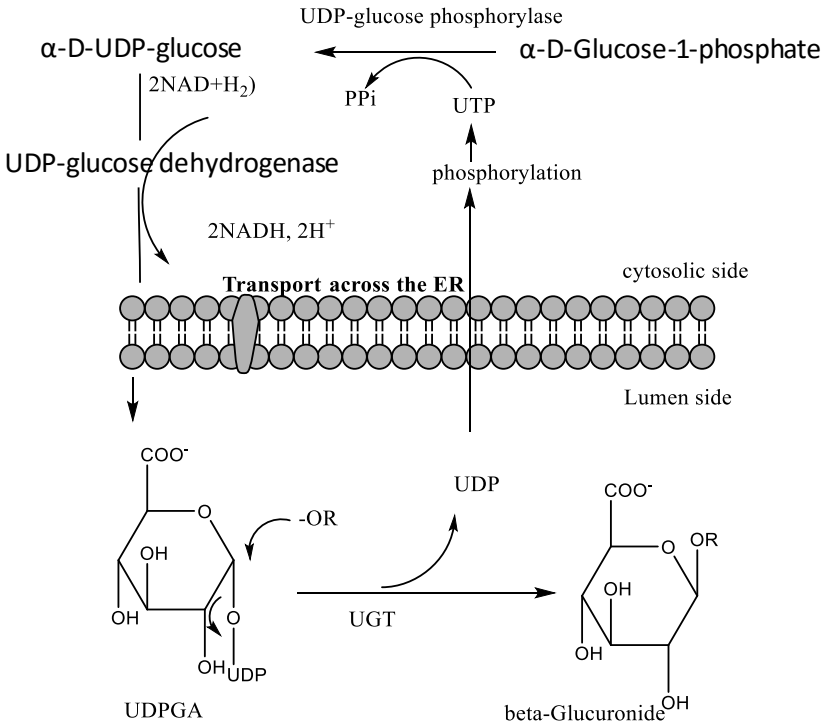

Figure 7. A depiction of the catalytic cycle of UGT enzymes is shown in the above diagram.[9]

UGTs can be particularly relevant to carboxylic acid containing compounds as the deprotonated oxygen can readily attack UDPGA via a S_n2 reaction. However, glucuronidation of carboxylic acids results in the formation of acyl glucuronides.[7,9,10,11,12] Acyl glucuronides are susceptible to trans-acylation through nucleophilic attack from a nucleophilic amino acid residue such as lysine. Additionally, acyl glucuronides are able to undergo acyl migration and subsequent ring opening followed by glycation through a Schiff-base reaction with an appropriate amine containing residue (see Figure 8). Such

reactions are problematic as they may form modified proteins, potentially triggering a serious immuno-biologic response.[10,11,12]

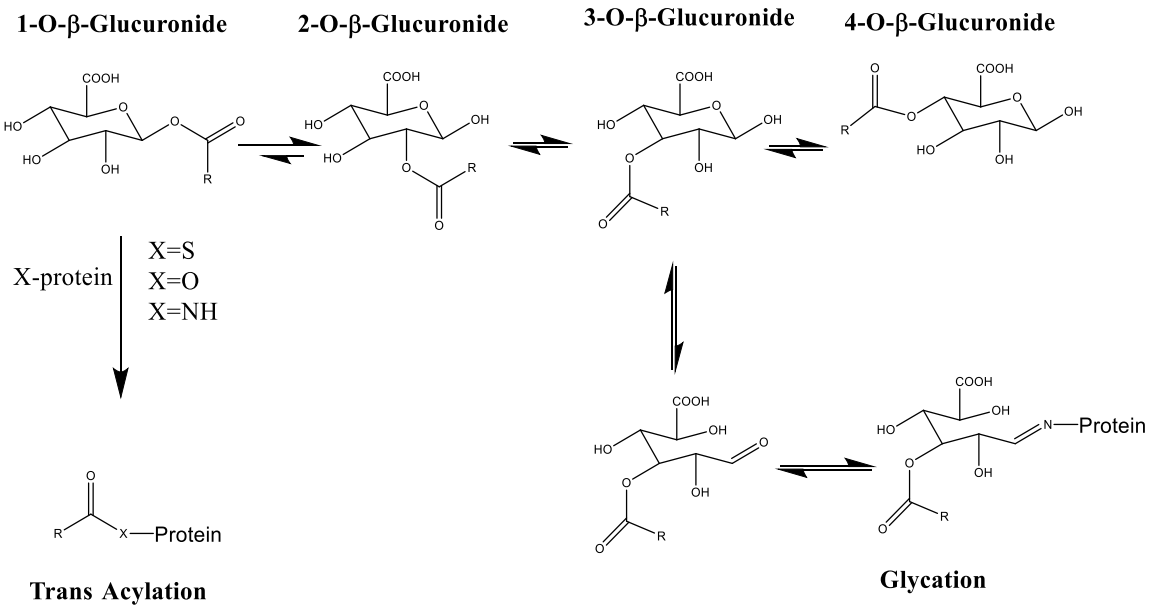

Figure 8. A mechanism for the reactivity of acyl glucuronides is proposed in the above figure. Acyl glucuronides are prone to attack from amino acids with a nucleophilic atom or subject to glycation via an acyl migration and subsequent ring opening. The ring opening exposes an aldehyde that is liable to Schiff-base reactions with a lysine or other amine containing residues. The resultant modified can potentially cause immunogenic responses.[10]

It has been reported that from 1960 to 1999, of the 121 drugs to be removed from the market, 17 of them contained carboxylic acids.[10] While this is certainly not a large percentage of compounds, many warnings have been given for over the counter NSAIDs (non-steroidal anti-inflammatory) such as diclofenac, indomethacin, and ibuprofen, all of which contain a carboxylic acid.[10-12] Many of the toxic responses caused by these drugs are believed to be related in part to the mechanisms mentioned above. Predicting whether an acyl glucuronide metabolite will contribute to toxicity is a complicated subject. Many factors such as stability of the metabolite, whether it circulates systemically, and how long it remains in circulation could contribute to its toxicity.[10-12]

1.4 *In vitro* Tools: Cryopreserved Hepatocytes and Microsomes

Suspended cryopreserved hepatocytes are isolated liver cells that are stored in liquid nitrogen. They possess the full complement of phase I and II enzymes as well as all necessary cofactors for metabolism.[9,13] Hepatocytes are often considered a benchmark assay for *in vitro* drug metabolism studies; however, they are not without detractions. Influx and efflux transporters can play a major role in how much of, or whether a drug can even reach metabolizing enzymes. In suspended hepatocytes, these transporters may not be properly polarized, or otherwise functional, hindering accurate *in vivo* metabolism prediction.[9,13,14] Additionally, hepatocytes are relatively expensive, making regular use somewhat prohibitive.

Microsomes are ERs that have been fragmented and separated via centrifugation at 100,000 xg. This results in formation of ER vesicles that contain many phase I and II enzymes, but lack many of the necessary cofactors such as NADPH and UDPGA needed for enzymatic activity.[13,14] Microsomes are robust, versatile (provided the necessary cofactors are added), and relatively inexpensive. For these reasons, microsomes are a mainstay for *in vitro* drug metabolism studies.[7,14]

Using microsomes for *in vitro* studies can be problematic for compounds that are heavily metabolized via glucuronidation, because UGTs are located on the lumen portion of the ER where they are not exposed to potential substrates (see Figure 9).[15,16,17,18]

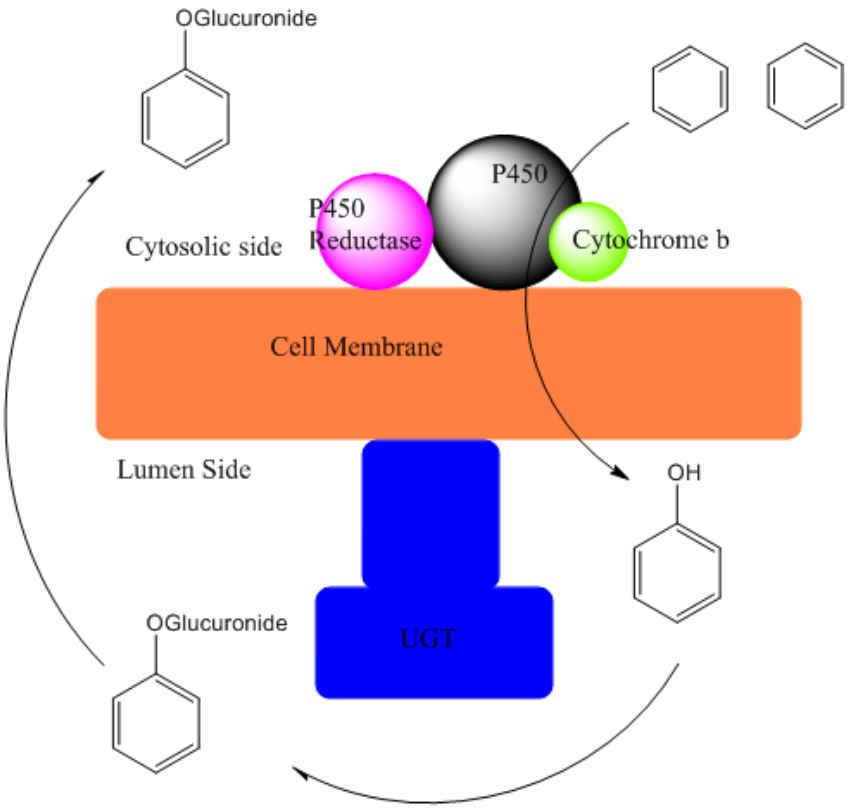

Figure 9. In the above figure both P450 and glucuronidation activity are shown; however, P450 is located on the cytosolic side of the ER and UGT is on the lumen side; substrates must first pass through the cell membrane to bind to the UGT enzymes.

Many strategies have been employed to release the latent potential of microsomal UGTs such as detergents to better predict metabolism for compounds that are substrates for UGT enzymes. However, harsh methods like these often harm other relevant enzymes such as P450 activity.[14,15] Newer methods typically employ the peptide antibiotic alamethicin. Alamethicin quickly forms regular size pores in microsomes, while leaving P450 functional activity intact.[15,18]

In vitro studies are common in drug discovery and development. When testing preclinical species, many PK parameters such as clearance can potentially be explained or estimated by determining the rate of metabolism in microsomes and hepatocytes.[14] These predictions can be further refined if specific enzymes responsible for a compound's metabolism can be identified. Additionally, reactive metabolites formed in preclinical species can be evaluated to see if they form in human microsomes or hepatocytes.[9,14]

1.5 Principles behind LC/MS

1.5.1 Chromatography Theory and HPLC and UPLC Applications

Accurately describing drug disposition requires bioanalytical techniques capable of separating and detecting the parent compound as well as potential metabolites. A compound can have many metabolites all with varying physicochemical properties, requiring a robust separation method to characterize and quantitate them. Column chromatography techniques such as high performance liquid chromatography (HPLC) and ultrahigh performance liquid chromatography (UPLC) are the single most important separation methodologies used in metabolism identification and PK studies.[19,20]

Liquid chromatography (LC) separates compounds by their affinity to partition between the stationary and mobile phases of a column. Different compounds will vary in the rate at which they partition between the phases, resulting in differing elution times (retention time "rt") between compounds. The ability of a column to separate two or any number of compounds is dependent on its selectivity, which is a function of the differing partitioning coefficients of the respective compounds.

Selectivity is affected by both the column packing material and mobile phase composition (which can be adjusted to achieve desired selectivity). In drug disposition studies of small molecules, most columns used are reverse phase. These columns utilize a hydrophobic stationary phase (silica bonded to C5, C8, or C18 alkyl chains) and a polar mobile phase such as water: acetonitrile mixture. For these columns, hydrophobic compounds elute later than hydrophilic substances.[19-21]

A given drug may be metabolized extensively into many disparate metabolites with greatly varying retention factors, resulting in peaks that could elute with the solvent front, or conversely, some that elute late in the chromatographic run, causing significant broadening effects, resulting in poorer resolution with other late eluting compounds. To compensate for the elution time problem of complex mixtures, a gradient profile is often employed.[21] A gradient profile adjusts the mobile phase composition over time, and thus selectivity over time. For reverse phase conditions this means an initial mobile phase with low organic content, which is increased in a linear or stepwise fashion. Doing so changes the retention conditions of a column so that polar compounds are retained longer and lipophilic compounds elute sooner. This helps keep poorly retained compounds on the column longer, allowing for better separation, and reduces peak broadening of strongly retained compounds by increasing the organic content and pushing them off the column before they can spread out too much due to migratory effects. Under these conditions, optimal resolution of complex mixtures can be achieved.[21]

1.5.2 Principles of Mass Spectroscopy in Metabolism and PK Studies

Mass spectroscopy (MS) has become an indispensable analytical tool in drug discovery, especially in regard to drug disposition characterization.[22] Robust and sensitive, it is an invaluable method for detecting metabolites and quantifying drug levels in complex biological samples. A brief explanation behind MS principles and utility in ADME characterization will be discussed presently.

Mass spectroscopy coupled to HPLC or UPLC systems function by generating molecular ions in the gas phase from LC eluent entering the MS ionization source. Ions are then transferred to the mass analyzer portion of the MS system where they can be selected and manipulated according to their mass to charge ratio (m/z) and sent to the detector where the molecular weights and intensities of ions entering the detector can be deduced.[22]

Many types of MS systems are available, the suitability of which is dependent upon the application. In this work two types of mass spectrometers were employed: a Sciex API-4000 Qtrap and Waters Xevo G2 QToF. The API-4000 Qtrap is a type of triple quadrupole (QQQ) mass spectrometer while the Waters instrument is a single quadrupole coupled to time of flight mass analyzer (QToF). Both systems provide unique and complementary strengths that offset their respective limitations.

The API-4000 utilizes an electrospray ionization (ESI) source to generate molecular ions. ESI generates molecular ions by first aerosolizing the LC flow through capillary forces, then charging the molecules through application of a high electric field. Charged molecules in the aerosolized droplets are desolvated through continued exposure to ESI gases and heat, decreasing the droplet size over time. As the droplet size continues to shrink, ion repulsion increases until columbic repulsion results in ion ejection from the droplets into the gas phase. Figure 10 provides an illustration of this process.[20,21]

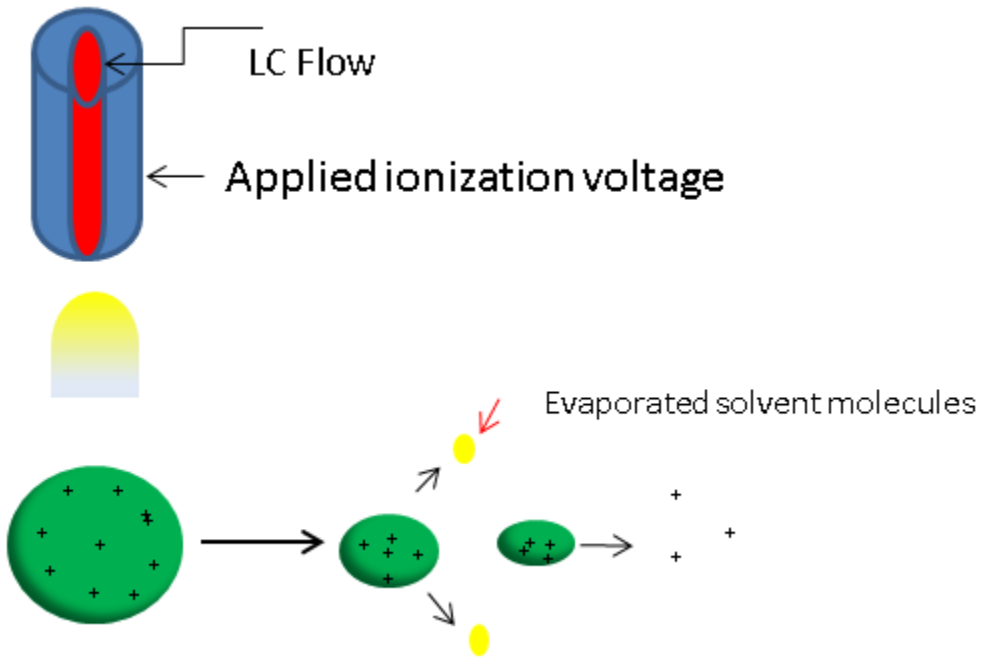

Figure 10. A schematic of the electrospray ionization process is shown above.

Ionization takes place in either positive or negative mode with generated ions being drawn to the mass analyzer portion via a combination of electric field and vacuum forces. The many disparate ions entering the MS migrate to the Q_1 quadrupole where they are exposed to a complex electromagnetic field, causing ions to adopt an oscillatory procession down the axis of the quadrupole; only ions with appropriate m/z ratios will maintain an appropriate trajectory to reach the second quadrupole, Q_2. Collison gas N_2 is injected into Q_2 and ions entering will collide with the gas, causing the molecules to fragment into daughter ions, which can be selected for in Q_3. As in Q_1, only ions with appropriate m/z ratios will reach the detector where the intensity (counts per second [cps]) will be recorded (see Figure 11).[21]

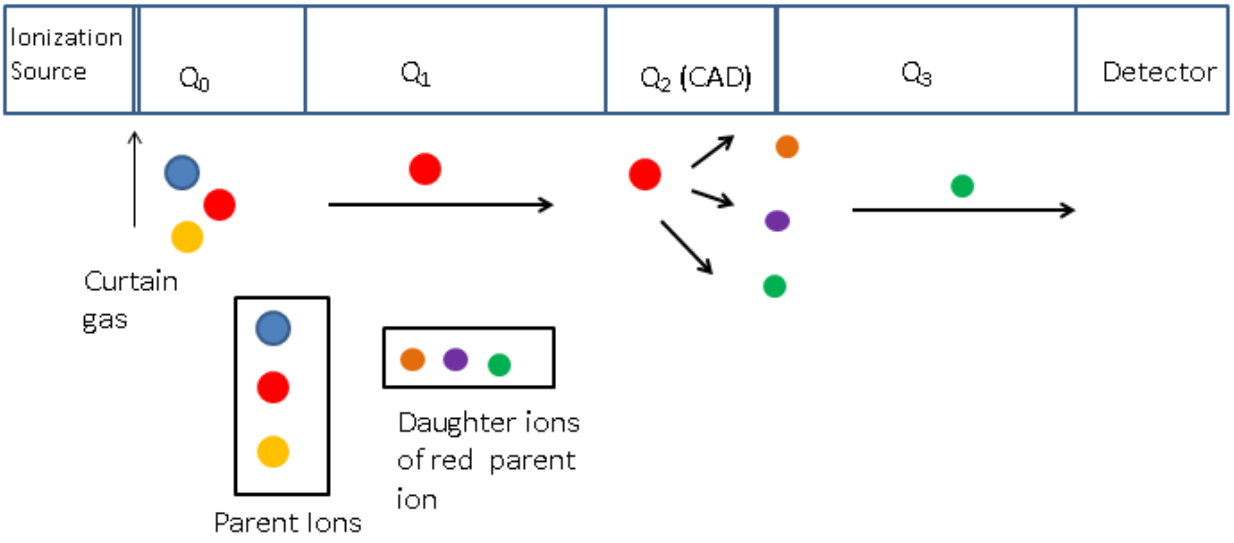

Figure 11. A schematic for multi reaction monitoring (MRM) using a QQQ mass spectrometer.

Ion fragmentation is an important aspect of triple quadrupole systems' selectivity since molecular ions fragment in a unique and predictable manner. Figure 12 illustrates a hypothetical fragmentation difference between two isobaric ions, an acetaminophen-hydrogen-adduct ion and 3-(2-hydroxyacetal)-benzenaminium ion. Both ions have the same amu (atomic mass unit), but acetaminophen fragments at the relatively weak amide bond, where the benzenaminium likely would not. This uniqueness in fragmentation allows ions with similar amu to be distinguished and monitored for in a highly selective manner. Figure 11 illustrates this process; as can be seen, many species of ions may be present in $Q_{0;}$ however, specific masses can be selected in Q_1 (red ion) and fragmented to daughter ions, which can be selected in Q_3 (green ion), then detected. This method of detection is referred to as multi reaction monitoring (MRM). Selection of a parent and its daughter ion is referred to as a transition; many transitions can be scanned for simultaneously when using MRM mode.

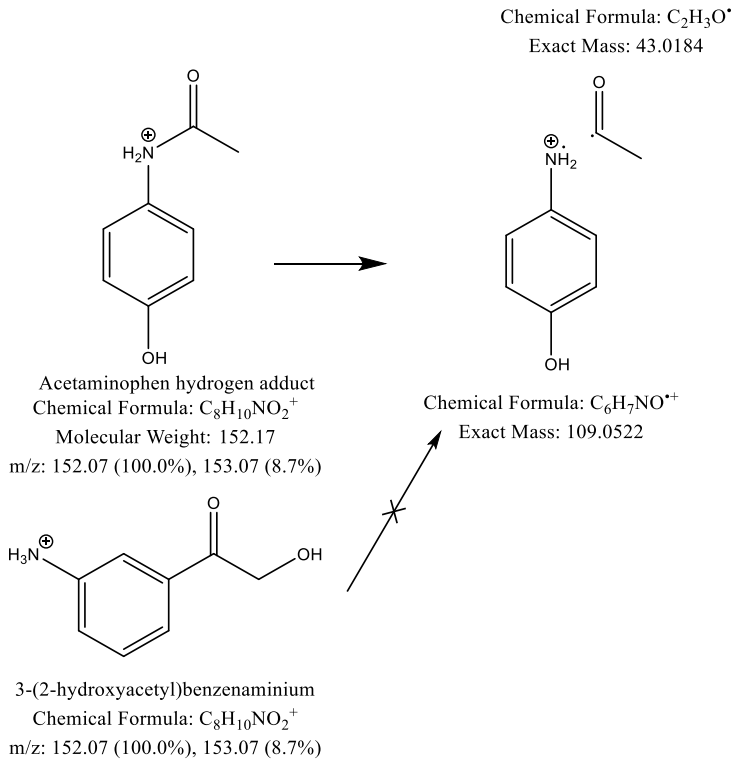

Figure 12. A hypothetical fragmentation pattern of two isobaric ions.

QQQ quadrupole systems excel in quantitation applications when using MRM scanning conditions. Typically, standard curves containing the compound(s) of interest are used to measure the analyte concentrations in samples. A peak response measured in cps is recorded for each known standard, and linear regression is used to generate a response curve based on the intensity of each standard response. This curve is then used to quantify unknown samples through measuring the magnitude of their response relative to the standard curve. Since biological matrices contain myriad substances, some of which may interfere with the ionization process, it is important to prepare standard curves in a similar matrix to those of the samples, to ensure similar ionization conditions.

Moreover, use of an internal standard (IS) is often employed (one with a similar structure and retention time is desirable) to help account for ion suppression as well as account for extraction efficiency during the sample preparation process. A well-chosen IS will have similar extraction ratios to the analyte of interest and will be subject to similar ionization suppression/enhancement effects. MRM is very sensitive, selective, and often capable of detecting compounds at very low concentrations.

Aside from quantitation, QQQ systems can be used for metabolite detection purposes. Since drug biotransformations modify a compound's molecular weight according to the specific type of biotransformation, MRM transitions incorporating these changes to parent and daughter ions can be used to monitor for specific metabolites in a sample.[20] Figure 13 gives a generic illustration of the process: here the parent unmodified ion is represented as a connected rectangle and oval, which fragments into rectangle and oval ions. Directly below the parent ion are metabolites which have undergone enzymatic modification indicated by the addition of an X and Y. These too will likely fragment similarly to that of the parent ion; however, the daughter ions will have amu values differing by the mass of X and Y respectively. By adding transitions that incorporate the mass changes caused by X and Y modifications, these metabolites can be detected and the location of biotransformation can be narrowed.

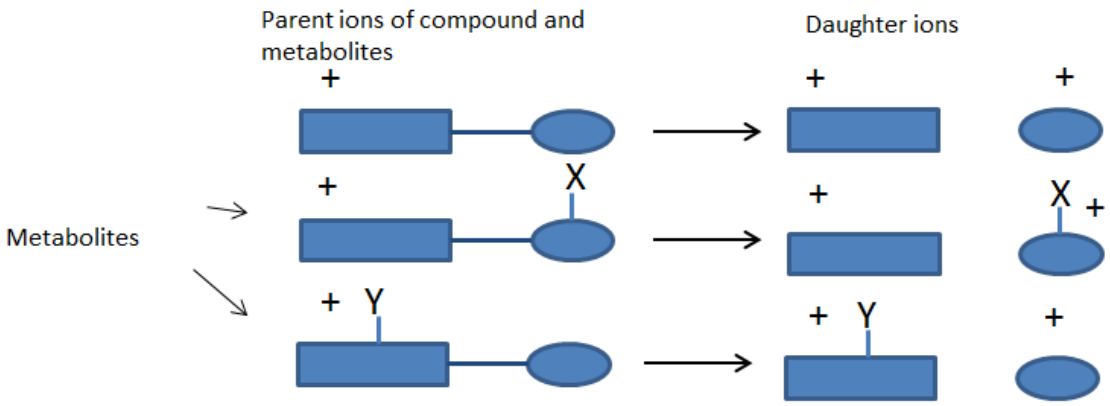

Figure 13. Use of MRM scanning mode with QQQ systems for metabolite identification.

QToF spectrometers function similarly to QQQ systems from the ionization source to the quadrupole; however, the method of selection differs significantly. As the name implies, QToF systems separate ions based on their time of flight. When analyzing for small molecules, ions typically have a single charge, meaning all ions have the same kinetic energy, but different velocities that depend on the mass of the ion (i.e. heavier ions will travel more slowly than lighter ions). Rather than filtering ions through electromagnetic fields and fragmentation, ion amu are deduced simply by the time it takes an ion to traverse the known distance to the detector.[21] This difference in selection imparts capabilities not present in QQQ systems, and makes QToF platforms ideally suited for metabolite identification studies.

Two of these attributes are high mass resolving power and accurate mass measurements. Mass resolution is the ability of a mass spectrometer to distinguish ions of differing molecular weight and is defined by an ion's MW divided by change in mass at ½ peak height (Equation 8).[23,24]

(8) $Resolving\ Power = mass/\Delta mass$

Mass accuracy is the ability of the mass spectrometer to measure an ion's true mass and is determined by measuring the mass error (the absolute difference between measured ion mass and actual mass). Accuracy is typically measured in parts per million (ppm) defined by Equation 9.[23,24]

(9) $mass\ error\ in\ ppm = \frac{mass\ error}{accurate\ mass} 10^6$

Accurate mass spectroscopy allows for a more certain identification of unknown metabolites, even in complex matrices such as bile and plasma.[24] An endogenous substance may ionize and have a very similar mass to a metabolite, but if the mass error is above the threshold of that mass spectrometer, it is not a metabolite.

1.6 Goal and Objectives

Telmisartan is an excellent candidate to assess the effect on dispositional changes caused by substitution of carboxylic acid with a tetrazolone. Telmisartan disposition across species is well documented and very similar across species.[25,26,27] In all tested preclinical species, telmisartan is predominately glucuronidated to the acyl glucuronide metabolite, then eliminated via biliary excretion into feces. All metabolism occurs through the UGT1A family in humans and preclinical species, with no P450 or other phase I or phase II reactions observed for *in vivo* or *in vitro* systems.[25]

Since telmisartan is cleared though metabolism of the carboxylic acid moiety, replacement of it with a tetrazolone may have a significant effect on the PK profile and metabolism. The tetrazolone analog R941000 could be excreted unchanged, glucuronidated, eliminated at a different rate, or undergo other biotransformations such as P450 oxidation.

Finally, SD rats were used as a model preclinical species since they are readily available and commonly used as an initial preclinical test species. PK parameters such as Cl, V, half-life, AUC (exposure), and C_{max} (highest plasma concentration) were determined using non compartmental analysis (NCA). Human *in vitro* metabolism was assessed using human cryopreserved suspended hepatocytes and liver and intestinal microsomes and compared to rat metabolism in the same *in vitro* platforms.

2.0 Experimental

2.1 Chemicals & Biological Materials

Telmisartan was purchased from TCI-America (Portland, OR), Bexarotene from LC Laboratories (Woburn, MA), Indomethacin from Alfa Aesar (Ward Hill, MA). Reduced NADPH salt, β-Glucuronidase, $MgCl_2$, UDPGA, DMSO, midazolam, propranolol, warfarin, and diclofenac were obtained from Sigma Aldrich (St. Louis, MO). Alamethicin was purchased from Santa Cruz Biotechnologies (Santa Cruz, CA). R941000, R941006, and R941007 (telmisartan, bexarotene and indomethacin tetrazolone analogs respectively) were synthesized and purified by Matthew Duncton at Rigel Pharmaceuticals Inc. (South San Francisco, CA). HPLC grade water and acetonitrile were purchased from Fisher Scientific (San José, CA).

Human and rat liver and intestinal microsomes were purchased from BD Genquest (San José, CA) and XenoTech (Lenexa, KS). Human and rat hepatocytes were obtained from XenoTech (Lenexa, KS). Rat plasma was purchased from Bioreclimation (Baltimore, MD).

2.2 Formulation Preparation

Both telmisartan and R941000 sodium salt formulations were prepared by dissolving the weighed material in 0.5 N NaOH and bringing up to appropriate volume in saline. The pH was then lowered to approximately 9.5 with 0.5 N HCl according to protocols detailed by Wienen (2007) & HAO (2012). Formulations were then dosed intravenously (IV) or orally (PO).[25-27]

2.3 Pharmacokinetic Studies

Sprague Dawley rats were dosed with either R941000 or telmisartan between 0.7-4 mg/kg. Formulations were administered either intravenously or orally, and blood was taken through the jugular vein at the following time points: 0.25, 0.5, 1, 2, 4, 6, 8, 10, and 24 h, centrifuged, and stored at -80 ^{0}C (as plasma samples) until ready to analyze. Samples were prepared by thawing at room temperature, and then adding 50 µl of plasma samples to 200 µl of IS containing acetonitrile to precipitate protein and extracting R941000 or telmisartan. A ten point standard curve ranging from 2-2000 ng/ml and quality controls (QCs) were prepared by adding 10 µl of appropriate concentration DMSO stock to 50 µl blank rat plasma, and then precipitating with 200 µl of IS containing acetonitrile, like the animal samples. Samples, standards, and quality controls

were then vortexed and centrifuged. Supernatant were then transferred to a 96 (1.2 ml) deep well plate and analyzed via a LC/MS API-4000 Q-trap (AB Sciex, Redwood City, CA) coupled with a Shimadzu 10Avp HPLC and SIL-5000 auto injector (Shimadzu, Pleasanton, CA).

In brief, samples were separated on an Essensil AF-C18 3µ 50x2.1 mm column using 0.05% formic acid in water (mobile phase A) and acetonitrile (mobile phase B) with a 0.4 ml/min flow rate. Initial column conditions consisted of 5% B for 0.5 min, then a linear increase from 5% B to 95% B over 2.5 min, followed by a 0.7 min wash phase (95% B), and then 0.7 min re-equilibration (5% B). Samples were ionized using an electrospray ionization (ESI) source on positive ion mode, with an ionization energy of 5500 V at 550 ^{0}C, and monitored using MRM mode. Telmisartan parent/daughter transitions were 515.2/497.2 amu with a 100 ms dwell time, 156 V declustering potential (DP), 45 V collision energy (CE) and 6 V exit potential (CXP). R941000 transitions are 555.2/484.2 amu, 100 ms dwell time, 71 V DP, 33 V CE and 6 V CXP.

The NCA pharmacokinetic profile of R941000 and telmisartan was assessed using Phoenix-WinNonlin software (Certara, Princeton, NJ).

2.4 Elimination Route Studies

Jugular vein cannulated SD rats were orally dosed with 3.5 mg/kg R941000 or telmisartan (n=3). Urine samples were collected at 0-6 h and 6-24 h, and feces were collected over a 24 h time period. Total volume and mass of urine and feces were recorded.

Urine samples were prepared and analyzed in exactly the same manner as plasma samples. Once the concentration in urine was determined, the total amount of drug in urine and percentage of dose could be calculated by multiplying the concentration by total volume (amount of compound) and then dividing by total dose received and multiplied by 100 for a percentage of dose excreted. Feces were first diluted in 10 ml of DMSO:water (50:50) and homogenized using a Biolabs (Manassa, VA) probe sonicator. Feces homogenate was then processed and analyzed in the same fashion as plasma and urine. The total amount of compound in feces was determined by estimating the DMSO:water dilution factor and multiplying it by the concentration of compound and total mass of feces collected. Percentage of dose in feces was determined by dividing the total amount found over total dose received multiplied by 100.

2.5 Hepatic Extraction Studies

Jugular and portal vein cannulated SD rats were dosed with 3-4 mg/kg R941000 or telmisartan and samples were collected at 0.5, 1, 2, 4, 6 h and stored at -80 ^{0}C. Plasma samples were then prepared and analyzed as previously discussed. Hepatic extraction was determined by Equation 10:

$$(10)\ \mathrm{HE} = \left(1 - \frac{\mathrm{AUCJV}}{\mathrm{AUCPV}}\right) * 100$$

Where HE is hepatic extraction, AUCJV is area under the curve for jugular vein, and AUCPV is area under the curve for portal vein.

2.6 Rat Bile Metabolite Identification Studies

Bile duct cannulated SD rats were dosed with 3-4 mg/kg of R941000 or telmisartan IV or PO and bile was collected from -1-0 h (pre-dose), 0-2 h, 2-4 h, and 4-6 h intervals and stored at -80 ^{0}C until ready to use. Samples were thawed, and aliquots from each time point were diluted 5-10 x fold in 0.1% formic acid containing water, vortexed and centrifuged to remove any non-dissolved bile components, and analyzed on a Waters Xevo G2 QToF, coupled to an Acuity UPLC system (Milford, MA).

Samples were then separated using a Phenomenex Kinetex C-18 100x2.1mm, 1.7µm UPLC column with an acetonitrile gradient (0.1% formic acid in water [A] and acetonitrile [B]) with a flow rate of 0.4 ml/min maintained at 35 ^{0}C. The column was equilibrated for 3 min at 15% B, then a linear increase from 15% to 60% B over 7.5 min, followed by a sharp increase to 95% B and a 3 min wash phase; finally, the column was re-equilibrated for 3 min at 5% B. Parent and metabolites were detected with the Acuity UPLC PDA detector and mass spectroscopy detector in survey ion mode (positive ion mode with ESI) with a mass range of 50-1000 amu and 200 msec scan time. The collision energy was set to a low (10 V) and high (30 V) collision energy and ramped from 20-60 V to optimize fragmentation of parent and daughter ions. Alternatively, the API-4000 Q-trap was used for metabolism identification, due to its greater sensitivity. Conditions used were similar to those used for plasma samples with the exception of a longer column (Phenomenex Luna C18, 5uM 150x3 mm column) and longer gradient method (20 min) with a 0.5 ml/min flow rate and 2 min equilibrium phase (5% B), 13 min gradient phase (5% to 95% B), followed by a 2 min wash phase (95% B) then 3 min

re-equilibrium phase (5% B). MRM transitions were set for 555.3/484.2 (R941000), 731.3/555.3 (R94000-glucuronide), 571.2/500.2 (oxidated-R941000), 515.2/497.2 (telmisartan), and 691.3/515.2 (telmisartan-glucuronide).

2.6.1 β-Glucuronidase

E. Coli β-glucuronidase was used to cleave *O*-glucuronides in bile samples by incubating 1,000 units of enzyme in bile samples buffered to pH 4 in sodium acetate buffer for four hours at 37 ^{0}C. Bile samples were then diluted 10x in 0.1 % formic acid containing water, vortexed, centrifuged, and analyzed on an API-4000 Qtrap using MRM parameters described previously.

2.7 Microsomal Stability Studies

Human and rat liver microsomes were thawed and diluted to a concentration of 1mg/ml microsomal protein in 100 mM phosphate buffer, pH 7.4, and aliquoted into 1.5 ml plastic micro-centrifuge tubes. A 1 mM DMSO stock containing test article (TA) was added to centrifuge tubes for a final TA concentration of 1 µM. The TA/microsomal suspension was aliquoted in a 96 deep well plate (in duplicate) and pre-incubated at 37 ^{0}C for 5 min. Following pre-incubation, a 40 mM stock of NADPH was added to the pre-incubated microsomes for a final concentration of 1 mM NADPH to initiate the reaction. Immediately following the NADPH addition, an aliquot from the TA/microsome solution was taken and quenched in acetonitrile (at 0 ^{0}C) containing internal standard (IS) for an initial time zero. Additional aliquots were taken at 5, 15, 30, and 45 min. Following

quenching, samples were diluted 3 fold in 0.1% formic acid in water, then vortexed, centrifuged, and analyzed via LCMS.

The relative stability of the TA was determined by tracking the disappearance of the TA over time by a linear plot of TA/IS peak area ratio. From the linear plot, the elimination constant, k, was estimated and the half-life of the TA was determined through Equation 11:

(11) $$t_{1/2} = -\frac{\ln(2)}{k}$$

2.7.1 UDPGA and Alamethicin Supplemented Human and Rat Liver and Intestinal Microsomes

The protocol for UDPGA supplemented and alamethicin treated microsomes was identical to the microsomal protocol with the exception of the following conditions: Microsomes were diluted to a final concentration of 1 mg/ml in phosphate buffer (pH 7.4) containing 1 mM $MgCl_2$ with the addition of alamethicin (at 50µg per mg of microsomal protein) and stored on ice for 15 min. Moreover, the reaction was initiated with the addition of UDPGA and NADPH (final concentration 5 mM and 1 mM respectively). Samples were quenched similarly to the previous microsome protocol at 0, 0.5, 1, and 2 h and prepared for analysis in the exact same manner as previously discussed. Samples were analyzed on the API-4000 Q-trap and monitored for TA and metabolites of TA.

2.8 Metabolite Identification through Cryopreserved Human and Rat Hepatocytes

Human and rat cryopreserved hepatocytes (HCH and RCH) were prepared following the protocol delineated by XenoTech for thawing cryopreserved hepatocytes (kits 2000, 2100, 2600).[28] Briefly, the hepatocytes were thawed in a water shaker bath at 37 ^{0}C for approximately 80 seconds and placed in solution A (Dulbecco's modified eagles medium [DMEM] and isotonic percoll), and 4.5 ml of tube B (DMEM) were added to hepatocyte suspension. The suspension was then centrifuged at 100 xg for 5 min at 37 ^{0}C, and the resulting supernatant was aspirated off. The remaining solution of tube B was added to pelleted hepatocytes, re-suspended, and centrifuged again at 60 xg for 3 min. Supernatant was aspirated off and the pelleted hepatocytes were gently re-suspended with a small volume of Krebs-Henseleit buffer (KHB). An aliquot of hepatocytes was stained with trypan-blue dye and then placed on a hemacytometer to determine cell viability. Once the number of viable hepatocytes were estimated, the remaining hepatocyte solution was diluted approximately $1.75x10^6$ cells/ml. Re-suspended hepatocytes were then added into 24 well polystyrene plates followed by a 0.75 x dilution with incubation media (pre-incubated to 37 ^{0}C) containing R941000, telmisartan, or blank (final substrate concentration 10µM). Cells were then incubated at 37 ^{0}C under 5% CO_2 atmosphere. Aliquots were then taken and quenched at 0, 2, and 4 h by adding to ice cold acetonitrile (1 x dilution). Four volumes of water containing 0.25% formic acid were then added to the quenched samples. HCH and RCH samples were then vortexed, centrifuged, and processed using the Waters Xevo G2 QToF and Acuity UPLC/MS.

2.9 Plasma Protein Binding

The percentage of R941000 and telmisartan bound to plasma proteins was determined using a Life Technologies Single-Use RED (rapid equilibration dialysis) device (Thermo Scientific, Research Triangle Park, NC). The assay was prepared by adding 500 µl of PBS (phosphate buffer saline), 1x solution to buffer side of plate, and 300 µl of plasma containing 2 µM TA. Samples were then mixed at approximately 800 rpm for four hours. Following the equilibration period, 50 µl plasma and buffer were removed from their respective wells and added to a 1.2 ml 96 deep well plate; 50 µl of blank buffer was then added to the plasma portion and 50 µl of blank plasma was added to buffer portion to normalize the samples; next, 300 µl of acetonitrile containing IS was added to each sample well, vortexed, and centrifuged. Supernatant was then transferred to a 96 deep well plate and analyzed via LC/MS in the same manner as the plasma PK samples.

3.0 Results

Results are divided into two sections: the first deals with pharmacokinetic and elimination behavior of R941000 and telmisartan through IV, PO, hepatic extraction, and elimination pathway studies; the second section looks at the metabolism of the two compounds in cryopreserved hepatocytes, and microsomes as well as *in vivo* metabolic profiling through analysis of rat bile from SD rats dosed with compound.

3.1.0 Pharmacokinetic Studies

Jugular vein (JV) cannulated SD rats were dosed IV with 0.70 and 0.79 mg/kg of R941000 and telmisartan, respectively, with three rats per study (n=3). Plasma samples were analyzed at the mentioned collection times from the PK experimental section for IV and PO studies. Figures 14 and 15 depict the IV PK profile of R941000 and telmisartan, respectively, with the upper and lower graphs representing the concentration over time and the linear plot concentration over time, respectively.

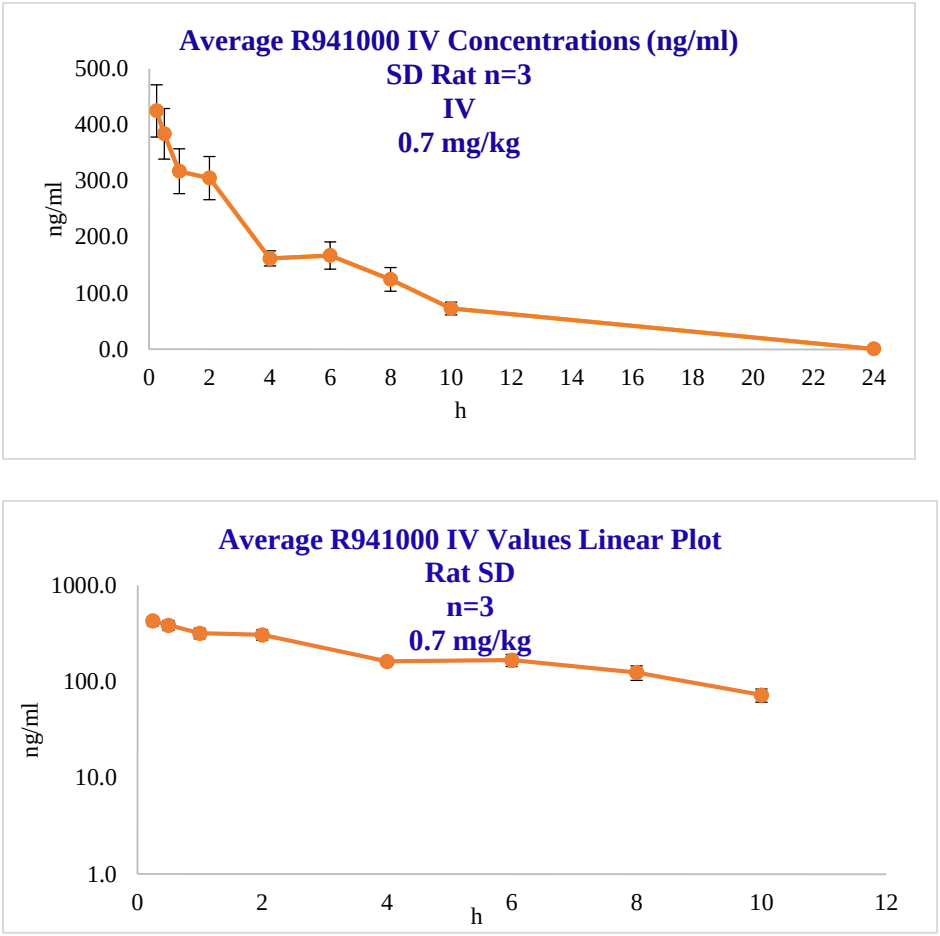

Figure 14. The top graph shows the PK profile of R941000 dosed via an IV bolus and the resultant concentration over a 24 h period. The lower graph depicts the linear plot of the same data.

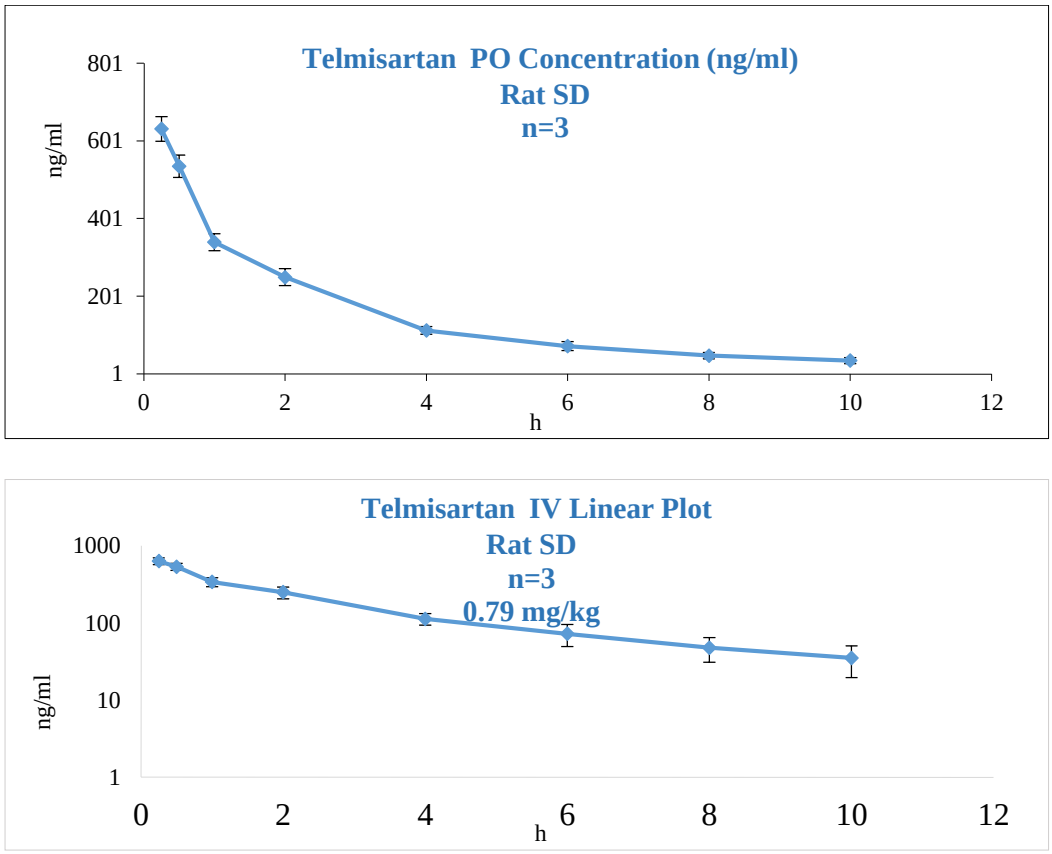

Figure 15. The top graph shows the PK profile of telmisartan dosed via an IV bolus and the resultant concentration over a 24 h period. The lower graph depicts the linear plot of the same data.

From NCA analysis, the PK parameters for both R941000 and telmisartan were determined, and are given in Table 1.

Table 1. IV PK parameters of R941000 and telmisartan

IV			**IV**	
R941000			**Telmisartan**	
0.7 mg/kg			**0.79 mg/kg**	
Variable	**Mean**	**SD±**	**Mean**	**SD±**
AUC_inf (ng*h/L)	2610	326	1850	258
AUC_last (ng*h/L)	2490	249	1830	245
Cl_pred (ng*ml/min)	4.51	0.691	7.23	1.09
t1/2 (h)	5.37	1.58	3.64	0.837
V_{ss} (L/kg)	1.67	0.242	1.59	0.14

Overall exposure for R941000 (2,610 ng/ml ± 326) is greater than telmisartan exposure (1850 ± 258), though it was given at an 11% lower dose. When the R941000 and telmisartan doses are normalized, the AUC of R941000 exceeds telmisartan by nearly 1.6 fold while Cl was reduced by a factor of 1.5.

SD rats were orally dosed with 3.5 mg/kg and 3.95 mg/kg of R941000 or telmisartan, respectively. Their plasma concentrations over 24 h were recorded and the resultant PK profiles can be seen in Figure 16 (R941000) and Figure 17 (telmisartan) with the oral PK parameters given in Table 2.

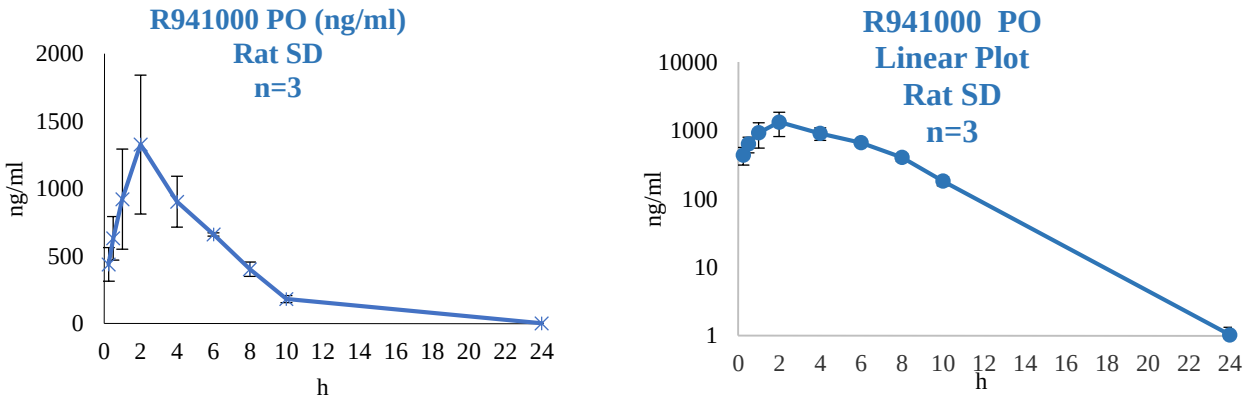

Figure 16. PK profile of PO dosed R941000.

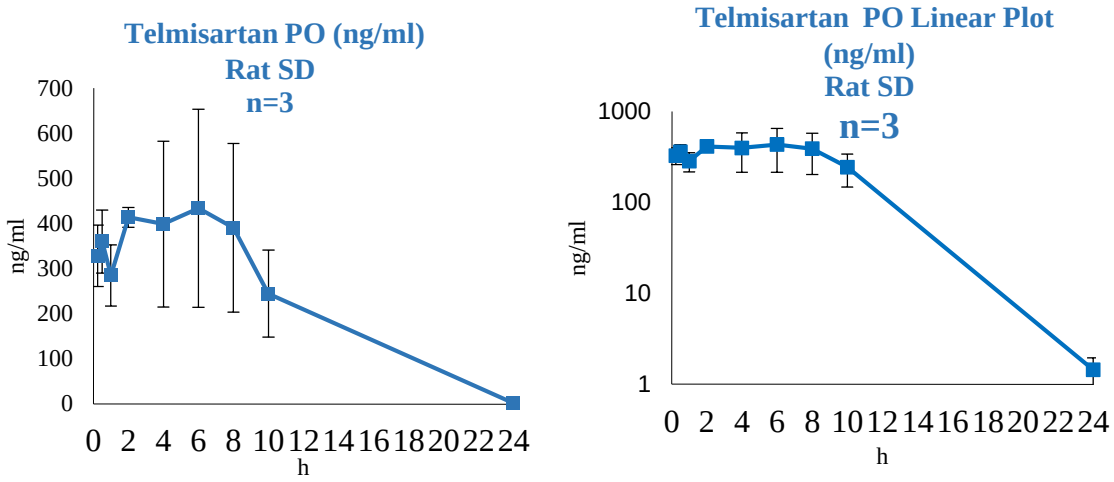

Figure 17. PK profile of PO dosed telmisartan.

Table 2. The PO PK parameters for R941000 and telmisartan.

PO			**PO**	
R941000			**Telmisartan**	
3.5 mg/kg			**3.95 mg/kg**	
Variable	**Mean**	**SD±**	**Mean**	**SD±**
AUC_inf (ng*h/L)	8440	1160	5480	1850
AUC_last (ng*h/L)	8420	1660	5460	1860
Cl_F_pred (ng*ml/min)	7.08	1.29	12.9	3.85
t1/2 (h)	2.65	0.320	2.55	0.856
Cmax (ng)	1330	515	506	158
%F	64.70%		59.20%	

As can be seen from the PK profiles, R941000 and telmisartan differ when administered through a PO route. R941000 has a clear T_{max} at 2 hours, but telmisartan has a plateaued profile with a large standard deviation and potential C_{max} values between 4-8 hours, depending on the animal. In addition to the relatively rapid absorption and definitive T_{max}, R941000 has a much greater C_{max}. From Table 2, it can be seen R941000 C_{max} is over 2.5 fold greater than telmisartan and increases to 3 fold when the doses are

normalized. Moreover, the overall exposure is 1.7 x greater than telmisartan, yet the half-lives are near equivalent.

A possible explanation of the prolonged telmisartan T_{max} may be due to its ability to undergo enterohepatic recirculation (conversion of the biliary excreted metabolite back to parent and reabsorption in the intestinal lumen).[25,26] Since telmisartan undergoes significant glucuronidation and biliary elimination, the *O*-acyl glucuronide metabolite in bile may serve as a telmisartan reservoir when endogenous gut β-glucuronidase hydrolyses the metabolite back to telmisartan.[25]

Samples were reanalyzed with MRM transitions monitoring for telmisartan-*O*-acyl glucuronide to see if enterohepatic recirculation may play a role in the observed telmisartan oral PK profile. Orally dosed samples showed a minor peak (2.47 min) eluted just prior to the major, parent peak (2.67 min) when observing the telmisartan MRM transition (see Figure 18). This observation was consistent with in source fragmentation of a glucuronide. In source fragmentation refers to ions fragmenting during the ionization process. Molecules with relatively weak bonds can undergo in source fragmentation, and in the case of an acyl glucuronide would be converted back to the parent ion. Since an *O*-acyl-glucuronide of telmisartan is more polar than its unmodified parent, it would elute first, showing two peaks when monitoring for telmisartan. When monitoring for the glucuronide metabolite a noticeable peak was observed at 2.47 min, the same as the in source fragmentation peak detected on the telmisartan MRM channel, providing evidence of an acyl glucuronide metabolite (Figure 18).

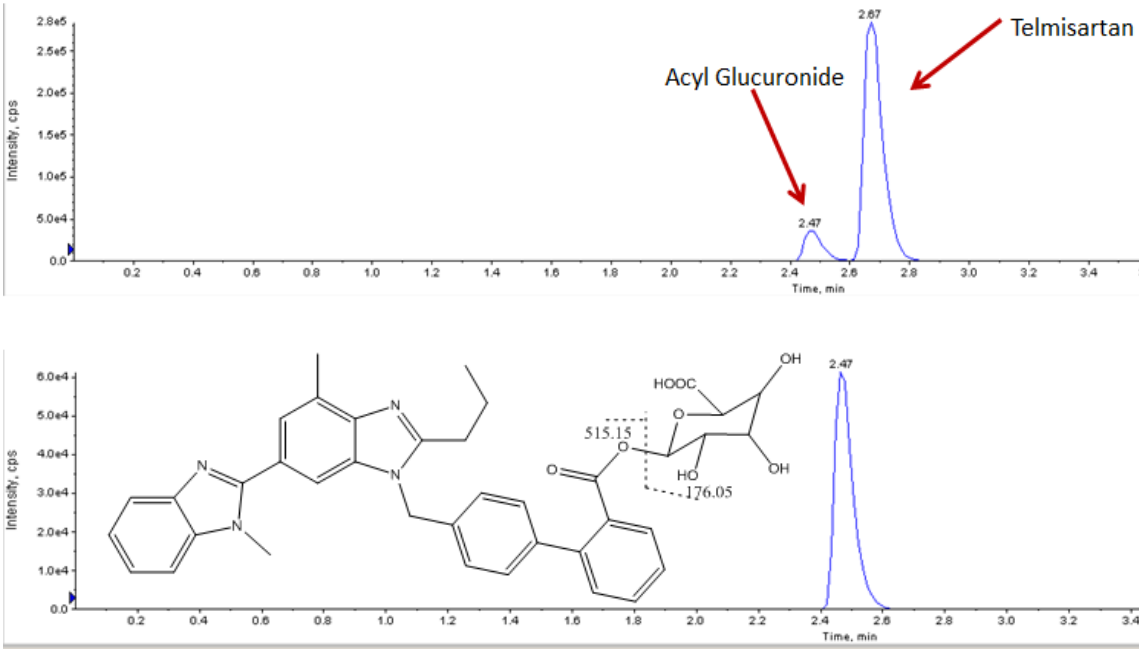

Figure 18. Chromatograms of telmisartan (top) and telmisartan-*O*-acyl glucuronide (bottom) MRM channels for orally administered SD rats at 0.5 h.

3.1.1 Hepatic Extraction

Telmisartan is glucuronidated in the GI track; however, the UGT1A family of enzymes responsible for glucuronidation becomes saturated with higher doses of telmisartan (greater than 1 mg/kg), and much of the glucuronidation falls to UGT1A enzymes in the liver.[25] Since the liver plays a prominent role in telmisartan metabolism, it was desirable to assess the magnitude of R941000 metabolism in liver through hepatic extraction studies. Determining hepatic extraction is performed by measuring drug concentration in both pre and post hepatic blood/plasma. This is often accomplished via jugular and portal vein cannulated rats. Since blood in the portal vein leads directly from the gut to the liver, measuring drug concentration in the portal vein is suitable for pre-hepatic concentration measurements.

Though somewhat distant from blood flow leaving the liver, drug concentration in the jugular vein is measured to determine the post hepatic concentration. In this study SD rats were dosed orally with either R941000 or telmisartan at approximately 3.5 mg/kg. Plasma samples were collected from both the jugular and portal veins from 0.5 to 6 h, with concentrations of compound recorded in Figure 19. In addition to the concentration profiles, Figure 19 contains the AUCs of both compounds as well as hepatic extraction ratios.

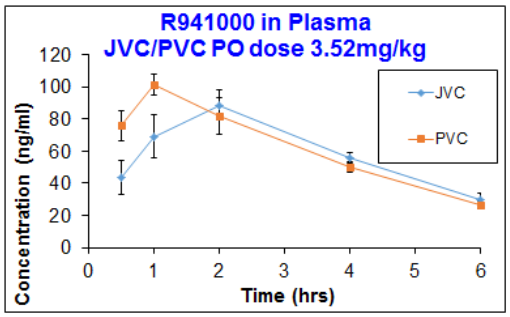

Summary R941000		
Plasma	AUClast (ng*hr/ml)	
	Average	SD
Jugular vein	348.00	62.10
Portal vien	364	66.10
Hepatic extraction ratio	0.044	

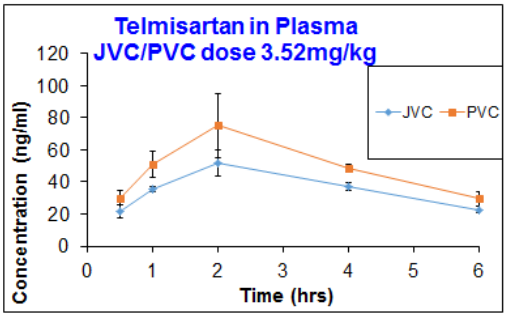

Summary Telmisartan		
Plasma	AUClast (ng*hr/ml)	
	Average	SD
Jugular vein	212	33.6
Portal vien	293	74.3
Hepatic extraction ratio	0.276	

Figure 19. Hepatic extraction ratios of R941000 (right) and telmisartan (left) are shown in the plot of compound concentration over time, and the percentage metabolized by the liver are shown in the tables listed below each graph. Both R941000 and telmisartan were dosed orally in SD rats (n=3) with concentration being measured over 6 h.

From the graphs, it can be seen for R941000 that the portal vein is initially higher in concentration than the jugular vein during the absorption phase (this is common for an orally dosed compound since all the drug is being absorbed from the gut and carried to the liver through the portal vein). During the terminal phase, however, there is little difference between the jugular and portal vein, suggesting minimal first pass effect in the liver. Indeed, only a 4% hepatic extraction was observed for R941000. Additionally, the PK profile for the HE study looked similar to the PO studies with rapid absorption and a clear C_{max}. Telmisartan possessed a later and lesser C_{max} than R941000, and had a HE of nearly 28% indicating a greater first pass effect from the liver.

3.1.2 Elimination Studies

Next, changes in elimination routes were assessed in SD rats, through collection of urine and feces over a 24 h period. Typically, mass balance studies using radiolabeled compounds to definitively determine when and how drug has left a body are employed. Unfortunately, radiolabeled compounds are very expensive and were not an option; however, a qualitative study would still provide valuable insight since any significant quantity found in urine would indicate a change in clearance route of the tetrazolone analog.

SD rats were dosed with R941000 or telmisartan at approximately 3.5 mg/kg. Urine and feces were collected over a 24 h period and the amounts in the respective matrices were determined as described in the experimental section. Results can be found in Table 3.

Table 3. Excretion amounts of R941000 and Telmisartan

R941000	**Telmisartan**
Urine < 1%	Urine < 1%
Feces approx. 40%	Feces approx. 50%

Approximately half of the oral dose was found in feces for both telmisartan and R941000 with only trace amounts detected in urine. Unfortunately, the samples were dosed orally, and 50% most likely correlates with the fraction of compound not absorbed by the gut (see Table 2, %F). Literature searches revealed most mass balance studies for telmisartan were conducted over 96 h, with over 90% of the compound excreted in feces the first 48 h.[25] While non-radiolabeled recovery studies are qualitative in nature, the low overall recovery may indicate much of the compound was still in the body after 24 h, metabolized, or that excreted compound was poorly extracted from feces samples. The lack of parent compound or metabolites found in urine over 24 h for both compounds suggests they both undergo biliary excretion.

3.2.0 Rat *In vivo* Metabolism: Searching for Metabolites in Bile

Compounds undergoing hepatic metabolism (such as telmisartan) can be transported and concentrated in the bile, where they can be concentrated and easier to detect.[25] Bile duct cannulated rats were orally or intravenously dosed with 3.5-4 mg/kg R941000 or telmisartan, and bile was collected at 4 time points, -1-0 h (pre-dose), 0-2 h, 2-4 h, and 4-6 h. Samples were then prepared as described in the experimental section, and then analyzed on either a Waters G2 Xevo QToF, or Applied Biosystmems API-4000 Qtrap.

A neat solution of 1 µM R941000 was prepared and run on the Waters UPLC-QToF platform, to determine the retention time of the molecule, the suitability of the gradient, and to elucidate the fragmentation pattern of R941000. An extracted ion chromatogram (XIC) shows a peak at 6.71 min (Figure 20, top). Analysis of the mass spectra at 6.71 min revealed numerous ions including a major ion with 555.260 amu, matching the hydrogen adduct molecular weight of R941000 with a mass error of 3.40 ppm. In addition, major fragments of R941000 were observed at 305.177, 251.094, and 208.076 amu (Figure 20, bottom). Figure 20 shows the likely portions of R941000 fragment ions 305.177 and 208.076 amu represent (generated using Excalibur software).

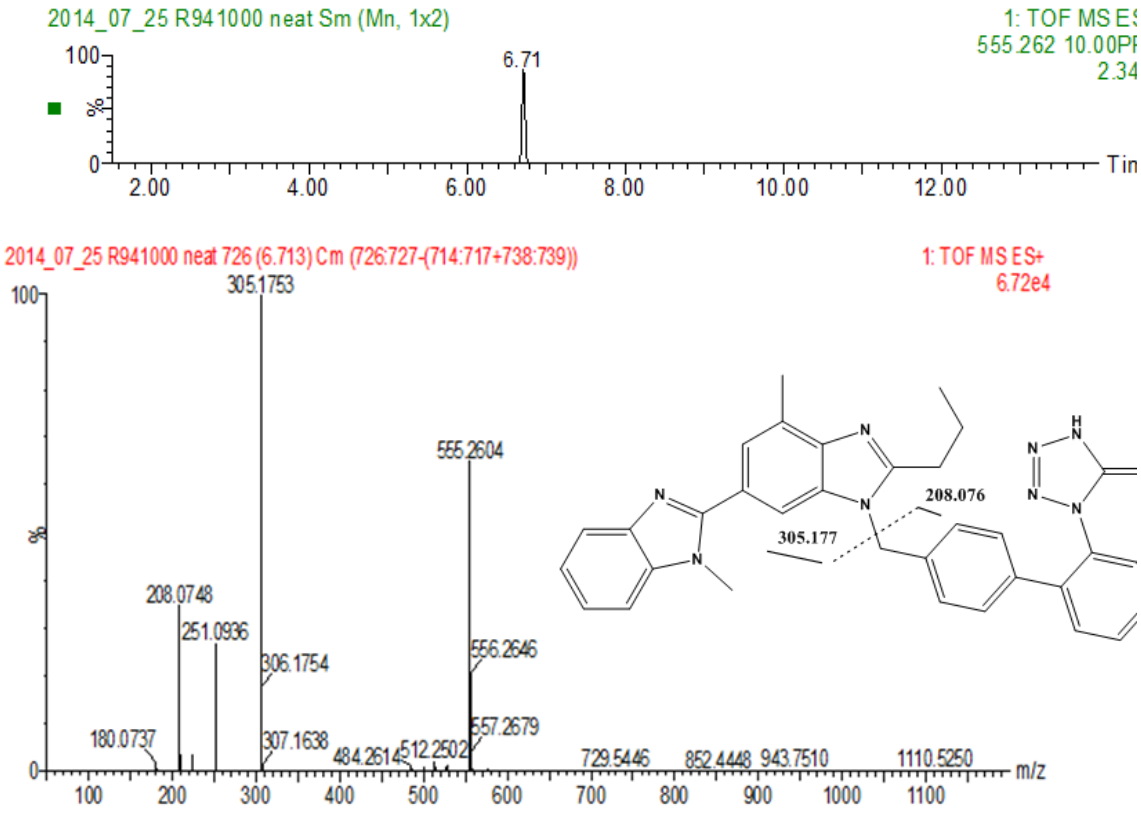

Figure 20. (Top) XIC chromatogram of 1µM R941000 in neat solution of 50:50 CH3CN:H2O. (Bottom) Mass spectra showing fragmentation pattern of R941000 from peak at 6.71 min.

Following the neat solution of R941000, the pre-dose through 6 h bile samples were analyzed using the same gradient and mass spectra conditions. XICs of bile samples for parent (R941000 hydrogen adduct) at 555.262 amu for all time points were performed and can be seen in Figures 21a-d. Distinct peaks were observed in the 2, 4 and 6 h samples, but absent in the pre dose sample.

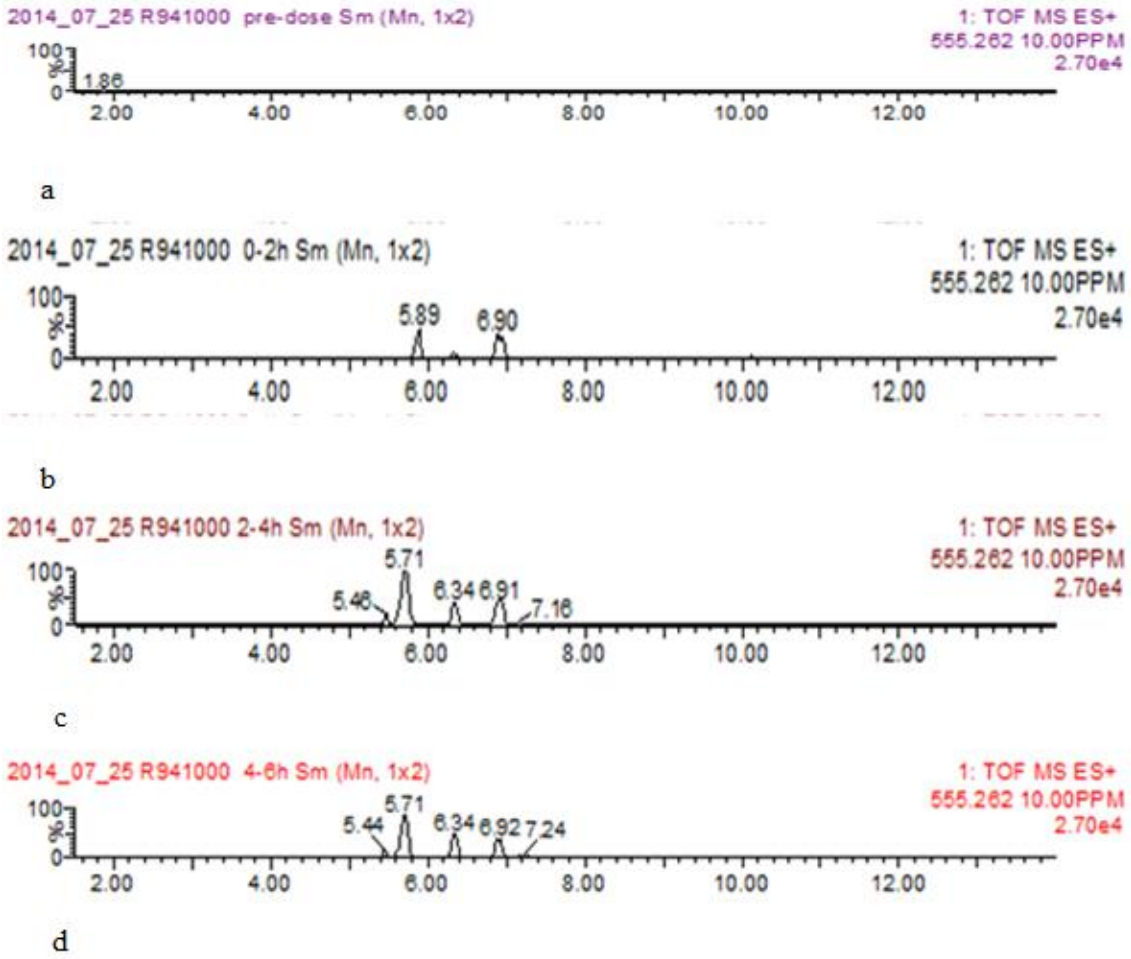

Figure 21. XICs of R941000 hydrogen adduct at 555.262 amu are shown for the pre-dose, 2, 4, and 6 h a-d samples, respectively.

In bile samples, the rt of R941000 shifted from 6.71 min in the neat solution to 6.91 min in the bile matrix solution; this is not uncommon for a complex matrix such as bile. Moreover, for the 2 through 6 h, multiple peaks of the parent 555.262 amu were observed, with increasing peak intensity of the earlier eluting species at the 4 and 6 h collection times. As previously discussed, observation of compounds with earlier retention times yet same mass can be indicative of in source fragmentation of a metabolite back to the parent structure.

An XIC of 731.293 amu (corresponding to a R941000-glucuronide [H^+] amu) resulted in the disappearance of the parent peak at 6.91 min, but remainder of earlier eluting peaks observed for XICs of 555.262 (Figure 22). For the 2 h bile sample (Figure 22 a) two distinctive peaks are visible at 6.32 and 5.88 min with a third peak appearing at about 5.4 min. XICs of the 4 and 6 h samples (Figure 22) revealed similar chromatograms.

Analysis of the mass spectra fragmentation patterns of the XIC peak at 6.3 min yielded a major ion with a MW of 731.291 amu with over a million cps. Additionally, the R941000 ion, 555.262 amu, was observed along with its characteristic fragments, 305.177 and 251.094 amu ions (Figure 23). Similar observations were made for the 5.8 and 5.4 min XIC peaks. Mass spectra of the 5.8 min peak yielded fragmentation patterns with the parent compound ion and characteristic fragmentation ion of 305.177 amu. The mass spectra of the 5.4 min peak had a mass error of 16 ppm from the glucuronide metabolite amu and therefore is not a metabolite.

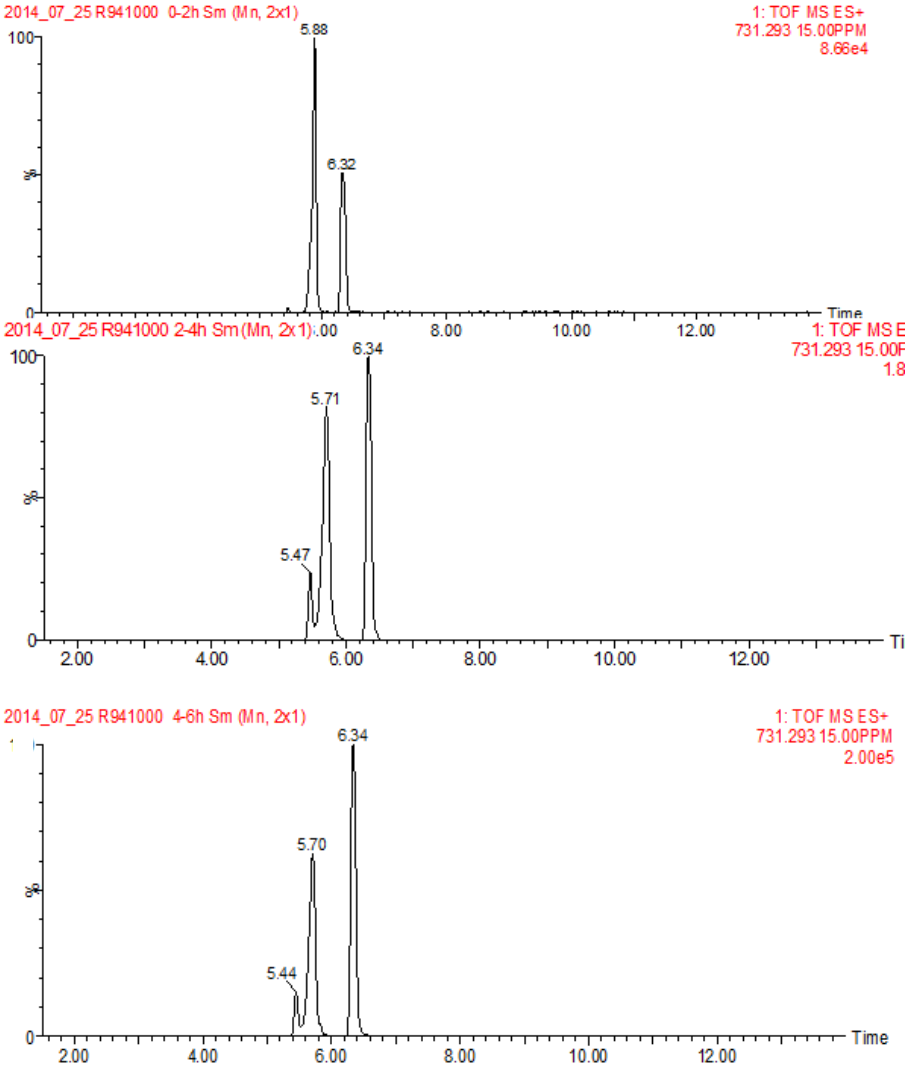

Figure 22. XICs of 731.29 amu from 2, 4, and 6 h bile samples are shown in top, middle, and bottom, respectively.

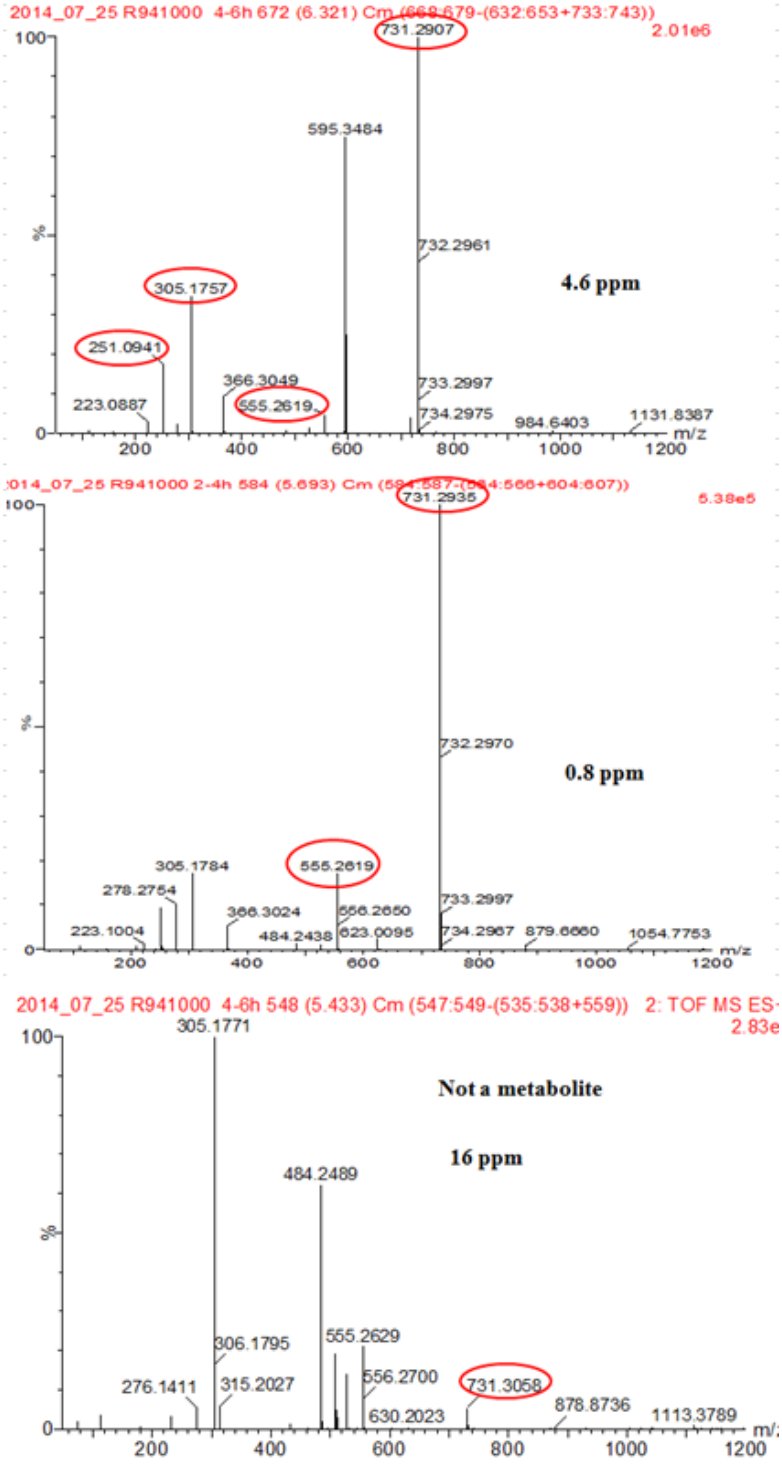

Figure 23. The above chromatograms show the mass spectra fragmentation patterns for the XIC (731.291 amu) chromatogram peaks at 6.3, 5.8, and 5.4 min (top, middle, and bottom, respectively) for the 4 h time point as well as their respective mass errors.

Analyzing the chemical configuration of R941000, two glucuronidation sites are apparent on the tetrazolone. The tetrazolone can tautomerize and exist in the enol or keto form, revealing either a nucleophilic oxygen (at the number 5 carbon on the tetrazolone ring) or nitrogen (number 4 nitrogen on the tetrazolone ring), depending on the tautomer. Either the oxygen or nitrogen can attack the electrophilic carbon on position one of the glucuronide, displacing UDP in an S_N2 type reaction, forming either an *O*- or *N*-glucuronide (Figure 24).

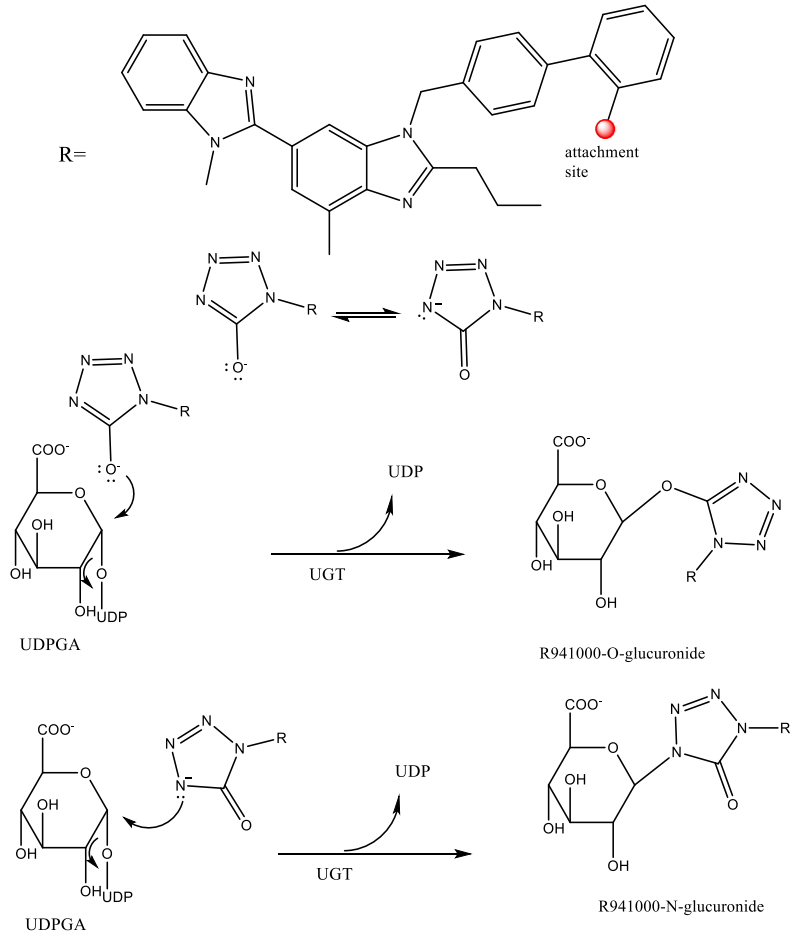

Figure 24. Tetrazolones can tautomerize between the keto and enol form, revealing two nucleophilic atoms capable of displacing UDP in an Sn2 attack forming an *O*- or *N*-glucuronide.

β-glucuronidase was next employed to test if the observed glucuronides corresponded to *O/N*-glucuronides. *N*-glucuronides are stable to β-glucuronidase while *O*-glucuronides are readily cleaved.[29,30] The API-4000 was chosen for analysis of the samples, due to its excellent sensitivity. The parent eluted at 10.81 min, preceded by a peak at 10.13 min, a minor peak at 9.59 min, and a second major peak at 9.29 min. The results of these experiments are shown in Figure 25, where the XICs of the R941000-glucuronide metabolites are shown for the 2-4 h bile time point without (top) and with (bottom) incubation in β glucuronidase at 37 ^{0}C. As can be seen, incubation of the rat bile with β-glucuronidase resulted in the disappearance of the 9.29 min peak, while the 10.81 min peak and minor peak remained. Therefore, the peak at 9.29 is likely to be an *O*-glucuronide, and the peak at 10.13 min an *N*-glucuronide.

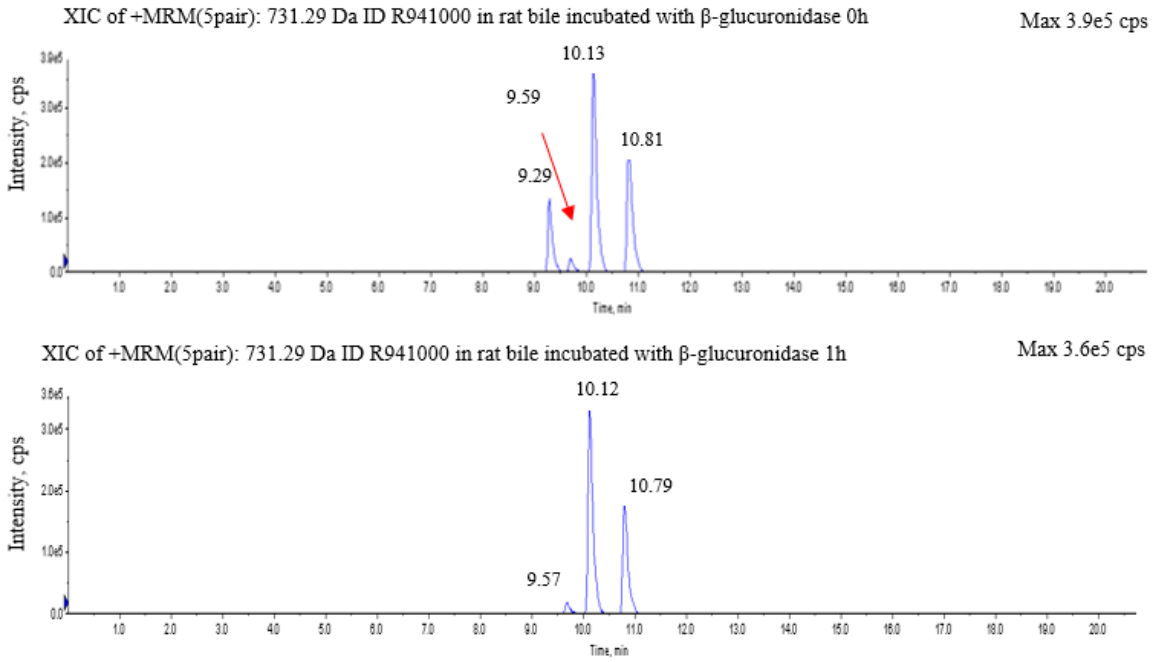

Figure 25. Top, XIC of 731.29 amu of rat bile 2-4 h after being dosed with R941000; bottom, XIC of 731.29 amu after 1 h incubation with β-glucuronidase at 37 ^{0}C.

After the potential identification of R941000 *O*- and *N*-glucuronides, a search for other less obvious metabolites began. The Waters QToF system was utilized for this purpose, due to its accurate mass and UV absorption capabilities. An initial check of the UV absorption chromatograms for all bile samples including the pre-dose was done at a 300 nm wavelength. A comparison of the pre-dose with later time points showed significant absorption at the glucuronide metabolite retention times, some absorption at the parent rt (6.91 min), and some additional peaks next to the parent (Figure 26 bottom). A wavelength of 300 nm was chosen to minimize non-specific matrix absorption, yet maintain absorption of parent and metabolites.

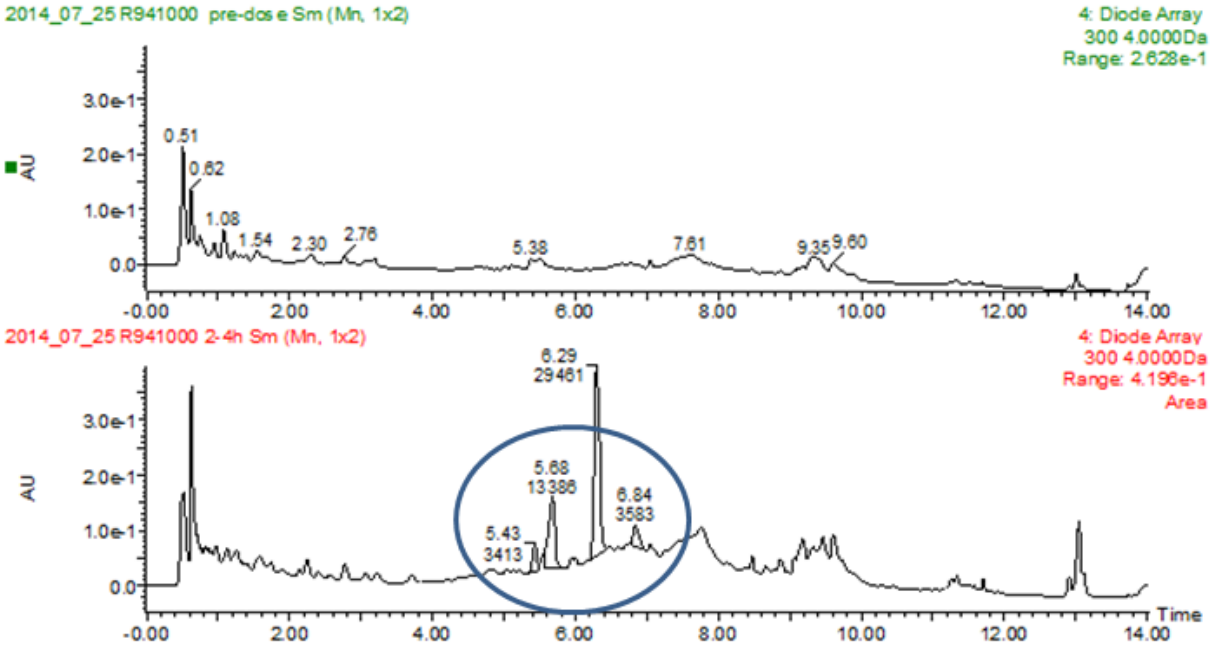

Figure 26. Top, UV of bile at pre-dose. Bottom, UV of bile at 2-4 h.

Next, XICs of common biotransformations were performed on all bile collection time points to determine if there were any other metabolites in the bile that either did not

absorb, or co-eluted with parent or other glucuronides. XICs of R941000 plus common biotransformation were searched for. These included oxidized metabolites and various phase II modifications, plus oxidation. However, the only other metabolites found were multiple singly oxidized species eluting at approximately 7.0, 6.8, and 6.5 min (Figure 27 top). Mass fragmentation patterns gave ions with parent +15.995 (addition of oxygen hereafter referred to as +16) for the above stated peaks (only shown for 6.8 min peak for 2-4 h bile sample [Figure 27 bottom]). As can be seen, there is a 208 amu fragment visible in Figure 27, indicative of the biphenyl portion of R941000 (Figure 28). In addition, there is a prominent 321 amu ion in place of the regularly observed 305 amu benzimidazole fragment of the molecule. This 305 +16 peak was observed for all oxidized species and is indicative of oxidation occurring on the benzimidazole portion of the molecule. Figure 28 illustrates the location of oxidation sites on R941000; however, due to the limited fragmentation of the parent compound it is hard to diagnose the exact location of biotransformation for each oxidized species. There are many potential sites of oxidation ranging from the alkyl side chains to aromatic rings.

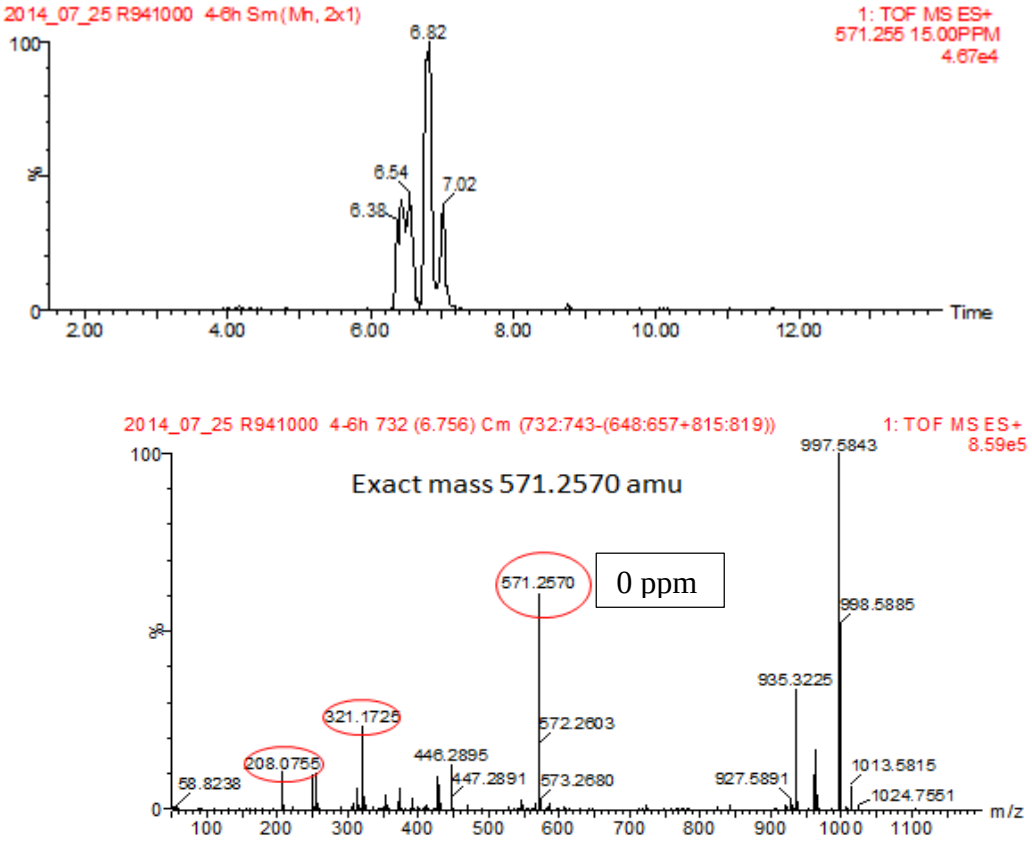

Figure 27. The top figure is the chromatogram showing the XIC of the parent +16 metabolite at 571.257 amu of the 2-4 h bile samples while the bottom shows the fragmentation pattern of the benzimidazole portion at 6.8 min.

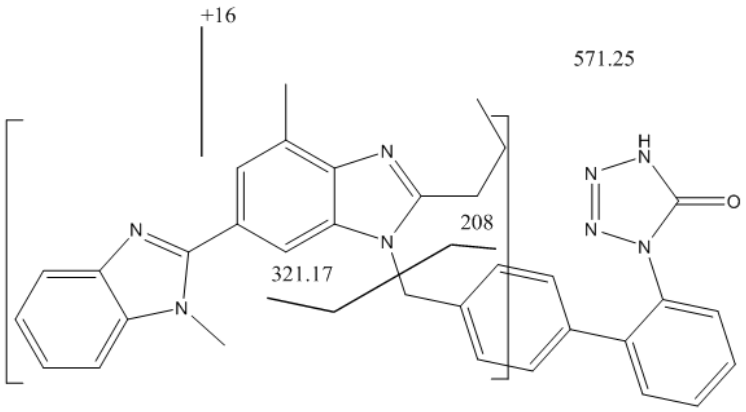

Figure 28. Potential sites of oxidation and resultant fragmentation patterns are shown above.

Due to the unavailability of radiolabeled R941000 and telmisartan, a qualitative approach using integrated UV absorption peaks was employed to estimate the relative amount of metabolites. UV peaks of parent and metabolites were integrated for each collection time and summed. UV absorption is used rather than integrated mass spectra data due to differences in ionization efficiencies of various molecules. A molecule that has relatively low abundance but easily ionizes may appear more intense through MS detection, than a highly abundant poorly ionizing molecule, giving a false impression of the relative amounts of ions. UV absorption, though, is likely to be more consistent across parent and metabolite species than MS since they would contain similar chromophores and absorption would be more dependent on quantity.

Summation of all metabolite peak integrations was done for all bile samples and recorded in Table 4 for each sampling time. The peaks observed at rt 5.68 and 6.28 min are the potential *O*-glucuronide and *N*-glucuronide, respectively. The relative absorbance of *N*-glucuronide by UV absorption ranged from 47.2% at 2 h to 56.6 and 56.2 for 4 and

6 h samples, respectively. Similarly, relative *O*-glucuronide absorbance ranged from a high of 24.0% (6 h) to 52.8% at 2 h. The peak at 6.84 min comprises both the parent and oxidized species since they were unable to be chromatographically resolved with the column conditions used while analyzing UV absorption. Parent and +16 metabolites abundance was 0.4% at the 2 h sample, but increased to 12.7% and 13.8% at 4 and 6 h, respectively. An unknown peak at 5.4 min showed a relative abundance at 6.1% at 6 h.

Table 4. Metabolite % by UV peak area.

UV Absorption Peak Area				
Metabolite	Unknown	*O*-glucuronide	*N*-glucuronide	Parent & +16
Time	5.4	5.68	6.28	6.84
0-2 h	-	13454	12018	10.45
2-4 h	-	16451	30292	6794
4-6 h	3712	14652	34203	8389
total absorbance @ RT	3712	44557	76513	15193
0-2 h %	0 %	52.8 %	47.2 %	0.04 %
2-4 h %	0 %	30.7 %	56.6 %	12.7 %
4-6 h %	6.10 %	24.0 %	56.1 %	13.8 %

3.2.1 *In vitro* Metabolism Studies

From characterizing the metabolite profile in rat bile, it was apparent glucuronidation plays an important role in R941000 metabolism and elimination; therefore, it was desirable to find *in vitro* systems that could be used to predict human metabolism. Since many similarities between human and rat metabolism exist, an *in*

vitro assay that mimics rat *in vivo* results may correlate to *in vivo* human metabolism. Two commonly employed systems for *in vitro* studies are microsomes and cryopreserved hepatocytes. Both hepatocytes and microsomes were used in the characterization of R941000 metabolism and will be discussed presently.

3.2.2 Rat and Human Cryopreserved Hepatocyte and Microsomal Studies.

Hepatocytes contain all phase I and II enzymes as well as the necessary cofactors for their proper function, and are considered a benchmark for *in vitro* metabolism studies.[14] For this reason, human and rat hepatocyte incubations were performed for *in vitro* assessment. Since glucuronidation appeared to be a major route of metabolism, telmisartan was used as a positive control to test UGT1A activity in the hepatocytes. Both R941000 and telmisartan were incubated at 10 µM for 0, 0.5, 1, 2, and 4 h using the same lot of rat and human hepatocytes. Samples were then analyzed using the Waters Xevo-G2 UPLC-QToF system for identification of metabolites. It should be noted that both human and rat hepatocytes were used for each compound; however, they both gave similar results and only human or rat data will be given as examples.

Incubation of telmisartan in human and rat hepatocytes resulted in the formation of the telmisartan-*O*-acyl glucuronide with no other metabolites being observed. Results are shown for human hepatocytes, and are given in Figure 29. The XIC of 515.24 (Figure 29 top) shows two peaks, one the parent (6.86 min), and presumably the in-source fragment of telmisartan-*O*-acyl glucuronide (5.61 min). Indeed, the mass fragment spectrum at 5.6 min yields a prominent ion of 691.275, with a mass error of 2.17 ppm for the telmisartan-*O*-acyl glucuronide; moreover, the telmisartan fragment at

515.243 amu (8.35 ppm) and characteristic 305 amu fragment are shown in the bottom portion of Figure 29, confirming the presence of the glucuronide metabolite and activity of UGT1A in the hepatocytes.

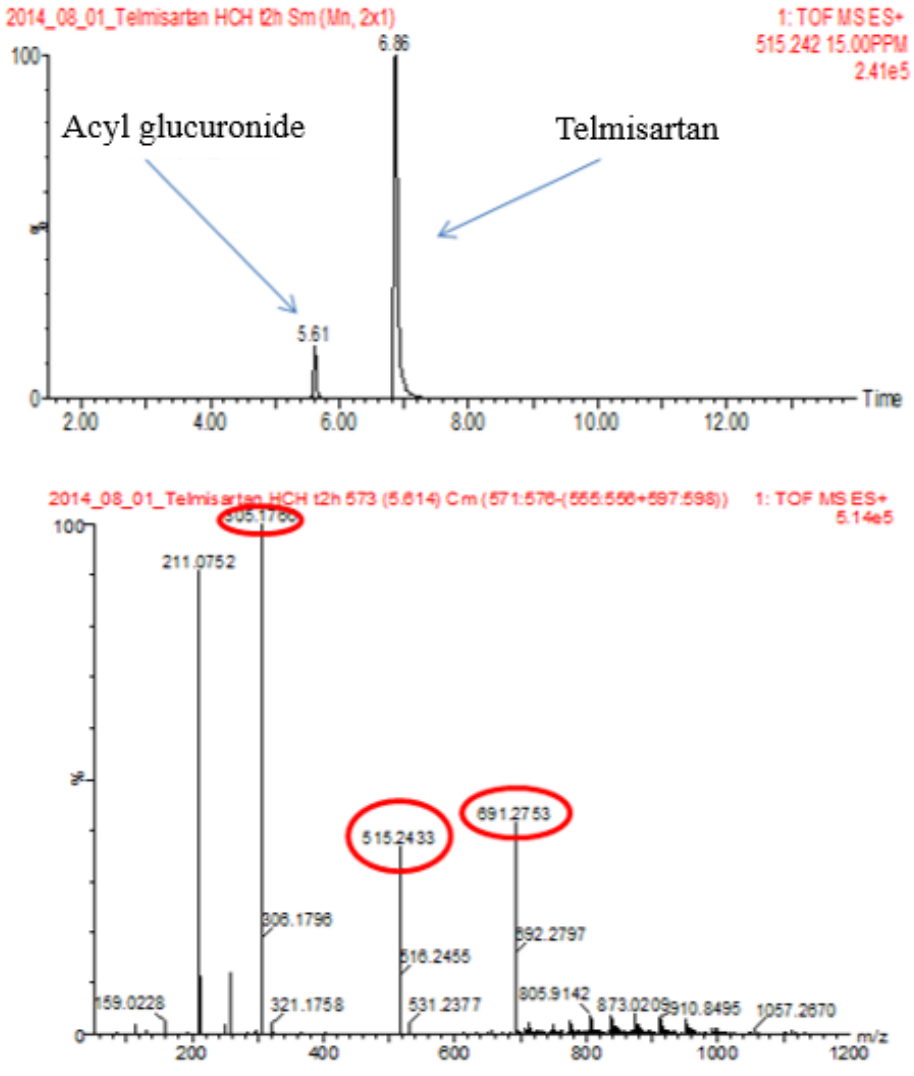

Figure 29. Telmisartan incubated in HCH for 2 h. The chromatogram (top) shows the XIC of telmisartan [H^+] with an acyl glucuronide peak and telmisartan peak. The mass fragmentation peak (bottom) of the acyl glucuronide at 5.61 min shows ions corresponding to telmisartan-*O*-acyl glucuronide [H^+] and characteristic fragmentation pattern.

Incubation of R941000 in human and rat hepatocytes yielded markedly different results from telmisartan. There were no obvious glucuronide metabolites when extracting the parent MW ion from the total chromatogram; additionally an XIC of 731.29 amu revealed no glucuronidated metabolites (Figure 30 top left). Analyzing the UV absorption of the spectrum revealed four peaks, with the parent at 6.6 min and three other minor peaks at 6.5, 6.2, and 5.8 min (Figure 30 top right). From the mass spectrum of each metabolite, it was determined they correlated with +16 metabolites of R941000, with the 6.5 min peak at 4 h incubation given as an example (Figure 30 bottom left). Further analysis of the fragmentation revealed a 321 amu ion, indicating oxidation of the benzimidazole portion of the molecule (Figure 30 bottom right). All peaks showed a similar fragmentation pattern, indicating oxidation occurs on the benzimidazole side of the molecule.

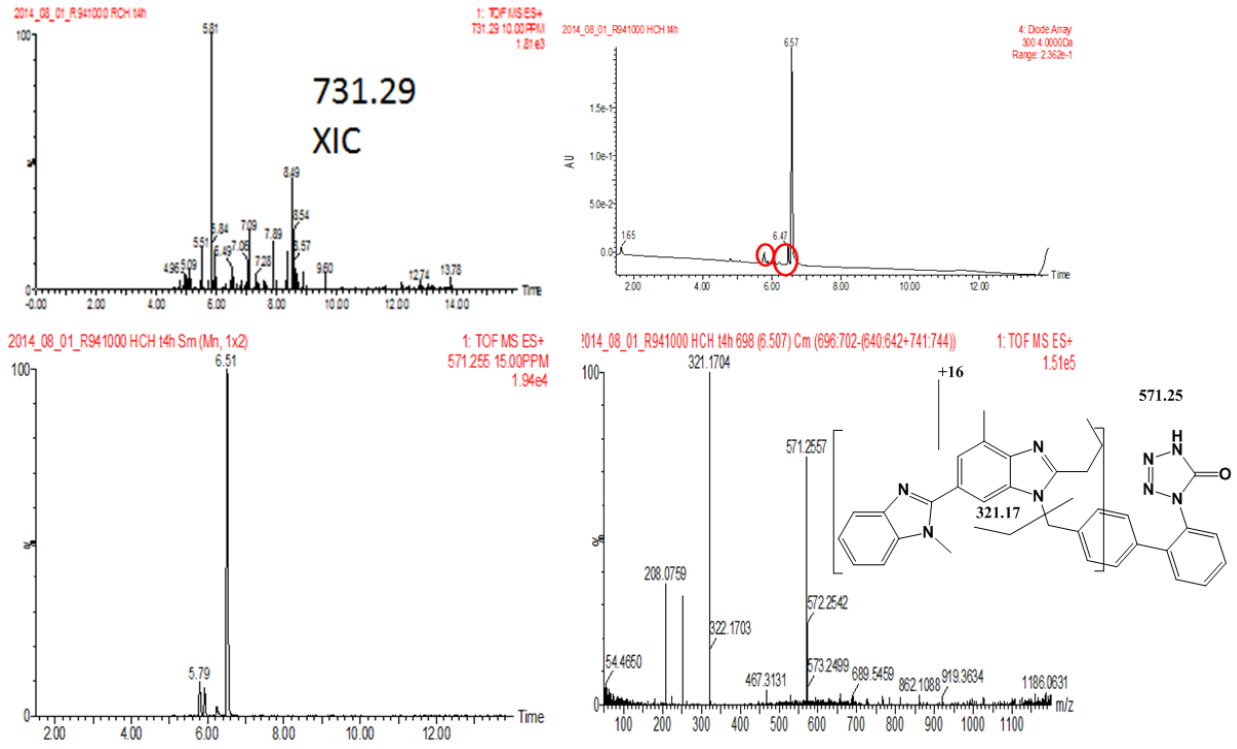

Figure 30. Results from the incubation of 10 µM R941000 with HCH at 4 h shown above. An XIC for the R941000–glucuronide (top left), UV absorption spectrum (top right), a XIC of 571.25 amu (bottom left), and mass fragmentation spectrum (bottom right) indicate only R941000 +16 metabolites observed on the benzimidazole portion of the molecule.

Incubation of hepatocytes displayed similar oxidation metabolism as was observed in bile, yet no glucuronidated species were observed. The hepatocytes did show UGT activity for telmisartan, so it was hypothesized there might be a permeability issue with R941000, either through passive mechanisms or an inability to be taken up by transporters. Telmisartan is a substrate for hepatic organic anion transporting polypeptide (OATP) OATP 1B3, and functional transporters may have facilitated its uptake into the hepatocytes, exposing telmisartan to UGT1A, whereas R941000 may have lacked this ability.[26] A method to expose R941000 to active UGT was desired to mimic the *in vivo* glucuronidation found in bile. Microsomes pre-incubated with the pore forming

polypeptide, alamethicin, supplemented with UDPGA and NADPH, was the methodology chosen to increase microsomal UGT activity.

A concentration of R941000 or telmisartan at 10 µM was incubated with alamethicin treated microsomes at a 1 mg/ml microsomal protein concentration with NADPH and UDPGA, respectively. Incubations were carried out from 0 to 2 h, and metabolite formation was monitored using the API-4000 Qtrap LC-MS system. Use of the triple quadrupole instead of the QToF was due to its excellent sensitivity and system availability. Additionally, a shorter 5 min LC run was utilized.

Telmisartan once again served as a positive control, and results are recorded in Figure 31, where all MRM channels are shown in one chromatogram. The red trace is that of the telmisartan MRM channel and the green trace is the acyl glucuronide metabolite. As can be seen there are two telmisartan peaks; the earlier eluting peak is that of the acyl glucuronide metabolite that underwent in source fragmentation, and the latter, the parent compound. Formation of the *O*-acyl glucuronide metabolite was confirmation that substrates such as telmisartan did indeed have access to the UGT enzymes and that at least UGT1A was active.

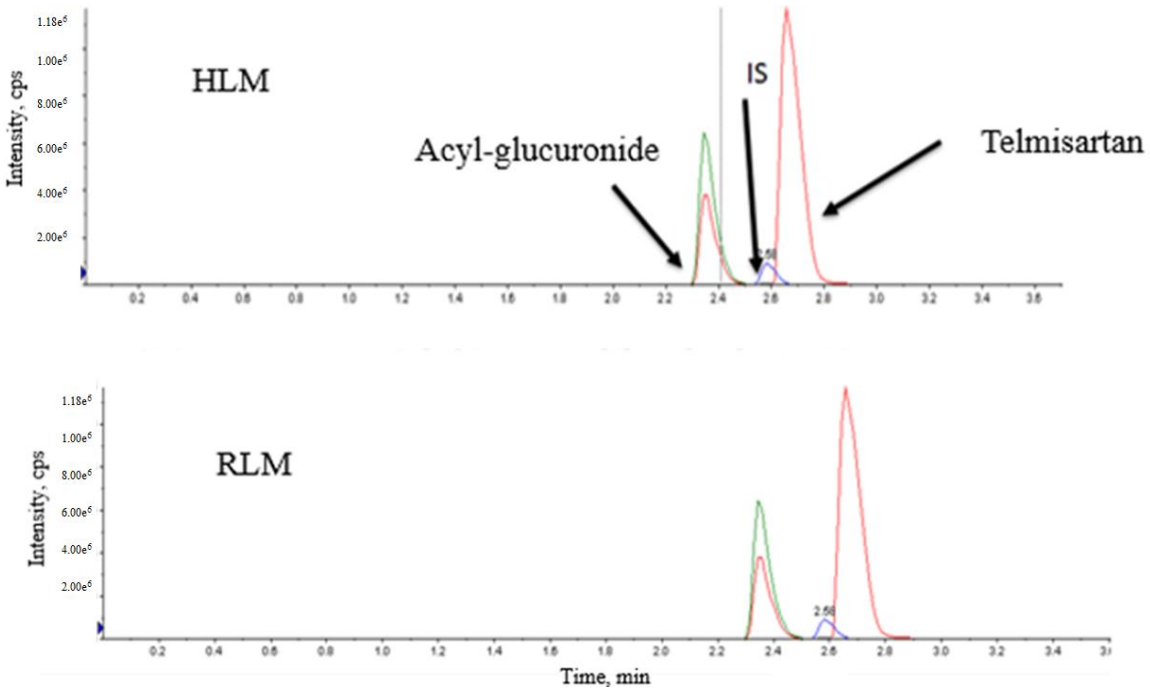

Figure 31. The top chromatogram shows the incubation of 10 µM telmisartan in HLM at 2 h in 1 mg/ml of microsomal protein treated with alamethicin. The red trace is the MRM channel for telmisartan, and the green is that of the acyl-glucuronide metabolite. The bottom chromatogram shows the results for RLM.

R941000 was incubated in treated HLM with the results recorded in Figures 32 and 33. Figure 32 shows the incubation results at 0 h with only parent and internal standard ions observed. Results at 2 h are given in Figure 33, where MRM channels for R941000, +16, and glucuronide metabolites are shown in top, middle, and bottom, respectively. R941000 had an intensity of about 10^6 cps, about twice the intensity of the main oxidized peak at 2.5 min. There were only two partially resolved peaks observed for +16 metabolites, one at 2.52 min, and the other at 2.45 min. This is likely due to the use of a shorter column with larger particle size (3 µm compared to 1.7 µm) and lower flow rate leading to a loss of resolution between the different metabolites. A glucuronidation metabolite appeared in its respective channel at 2.24 min; however, its relative abundance was low, with a peak intensity of approximately 2,000 cps. Moreover, only one peak was observed.

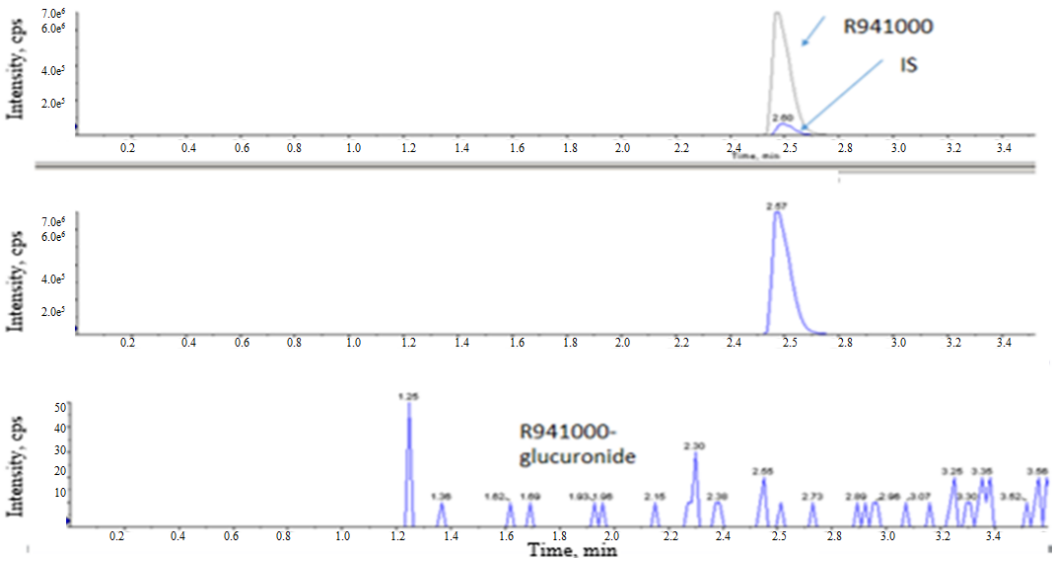

Figure 32. MRM of R941000 and its glucuronide metabolite in alamethicin treated HLM at time 0. MRM transitions for R941000 and IS (above), R941000 (middle), and glucuronide metabolite (bottom).

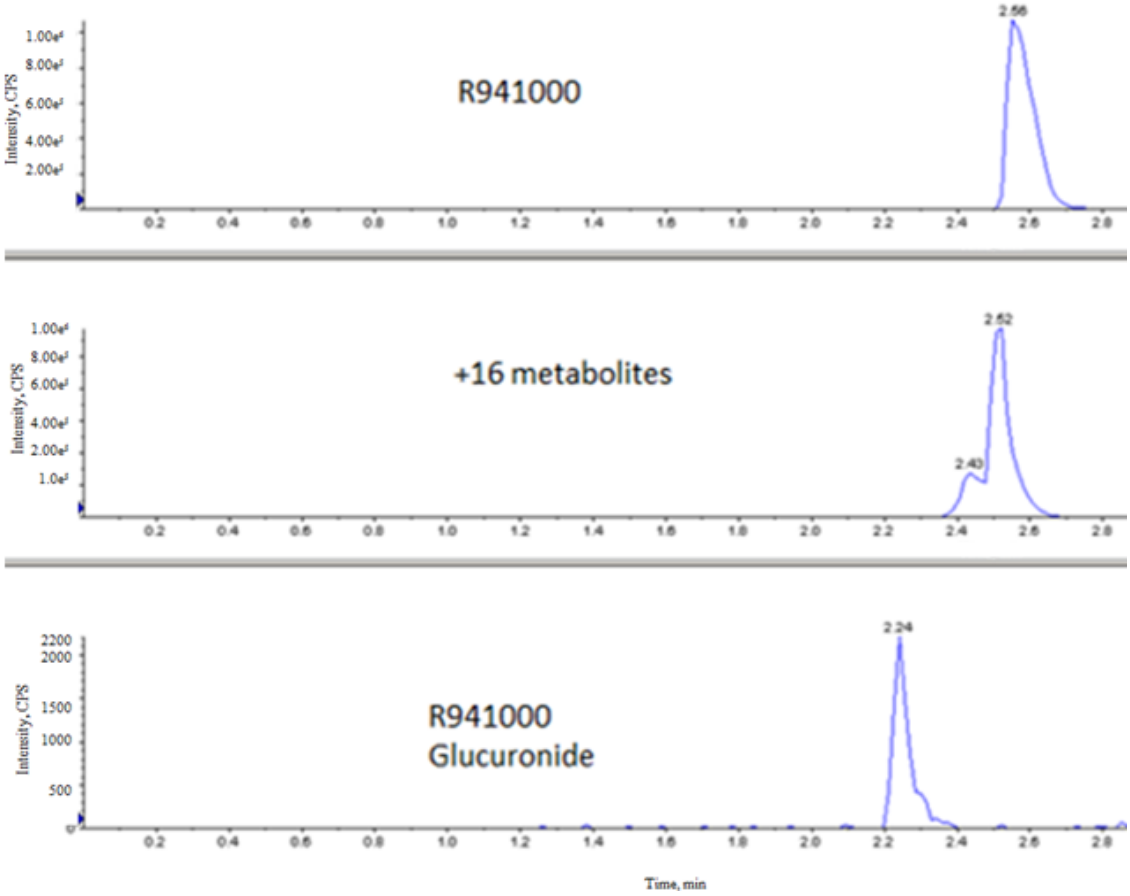

Figure 33. The above chromatogram shows the MRM transitions for R941000 (top), R+16 metabolites (middle), and the glucuronide metabolite transitions (bottom), with HLM at 2 h.

R941000 and telmisartan were incubated in alamethicin treated rat liver microsomes (RLM) under the same conditions as HLM (Figure 34); however, +16 metabolites were noticed, but no glucuronidation products were observed. Additionally, formation of oxidized species appeared anemic compared to HLM. These results were confusing since metabolite profiling in bile indicated glucuronidation is an important metabolism pathway. However, literature sources indicated that at low doses telmisartan is primarily metabolized in the gut, but UGT1A enzymes in the intestine get saturated at higher doses.[25] Additionally, *in vitro* data indicated telmisartan displayed an affinity for

intestinal microsomes. While limited in terms of capacity, the intestine does play an important role in telmisartan disposition at lower doses. Since hepatic extraction experiments showed little metabolism in liver for R941000, it was postulated that the gut may be the primary location of glucuronidation.

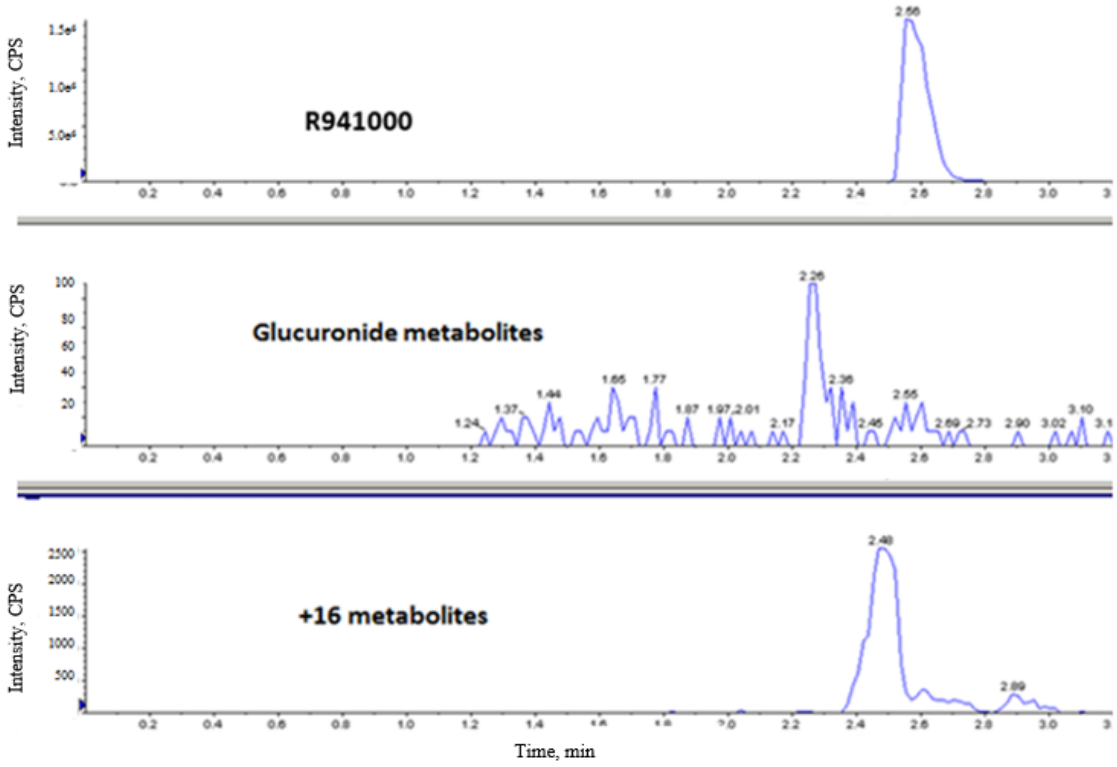

Figure 34. Incubation of 10 µM R941000 in alamethicin treated RLM at the 2 h time point. Above is the chromatogram of R941000 transitions; middle, the glucuronide MRM transition, and bottom, the +16 metabolites.

.

To test rat intestinal microsomal (RIM) activity, 10 µM R941000 was incubated in 1 mg/ml RIM protein treated with alamethicin in the same manner as RLM. Results are given in Figure 35, where it can be seen that a single glucuronide peak was formed, in addition to +16 metabolites. Like HLM, the relative abundance of glucuronides by mass spectroscopy appeared minimal, with only 1,500 cps being recorded.

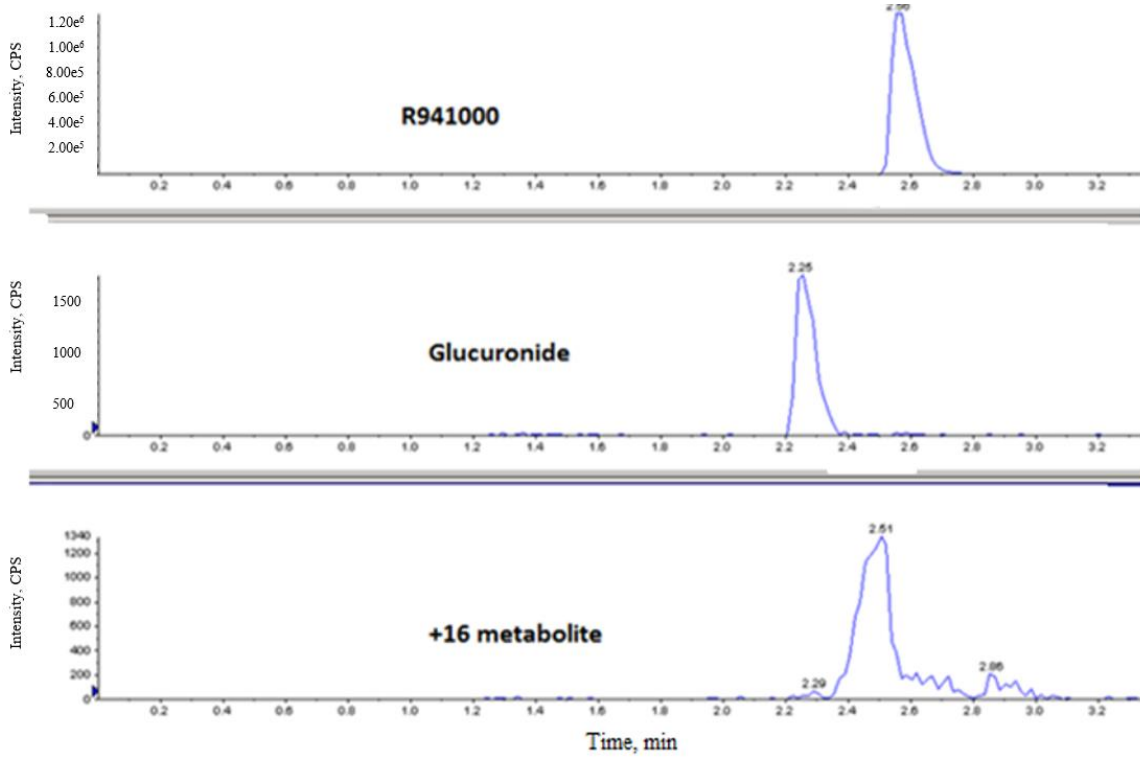

Figure 35. 10 µM R941000 incubated in alamethicin treated RIM for 2 h. The top chromatogram shows the parent R941000 channel, followed by the glucuronide (middle) and +16 metabolite (bottom) channels.

From the microsomal experiments, oxidation mechanisms appeared to be more relevant than glucuronidation activity, contrary to *in vivo* observations. Relative abundance by mass spectroscopy can be deceptive due to ionization efficiencies; additionally, other microsomal products may be forming that were not caught with the monitored transitions. To capture the importance of total phase I contribution to R941000 metabolism, microsomal stability assays were employed. For microsomal stability assays, a compound's disappearance over time is recorded and a half-life is established (see Equation 11). In this way, all contributing factors can be accounted for, and the importance of phase I activity can be established.

R941000 was incubated with HLM or RLM at 1 µM (reduced concentration to avoid saturation of enzymes) in 1 mg/ml protein over 45 min, with quenching times of 0, 5, 15, 30, and 45 min. Standards midazolam and propranolol were used for short and long stability controls (propranolol was metabolized quickly in rat; therefore, RLM lacked a long positive control). Results are recorded in Figures 36 and 37 (HLM, RLM) where midazolam had a half-life of around 3.5 min in HLM and RLM and propranolol 38 min in HLM and nearly 6 min in RLM. R941000 appeared stable with a half-life exceeding 45 min for both human and rat liver microsomes.

Compound	HLM
R941000	>45 min
Midazolam	3.71
Propranolol	38.1

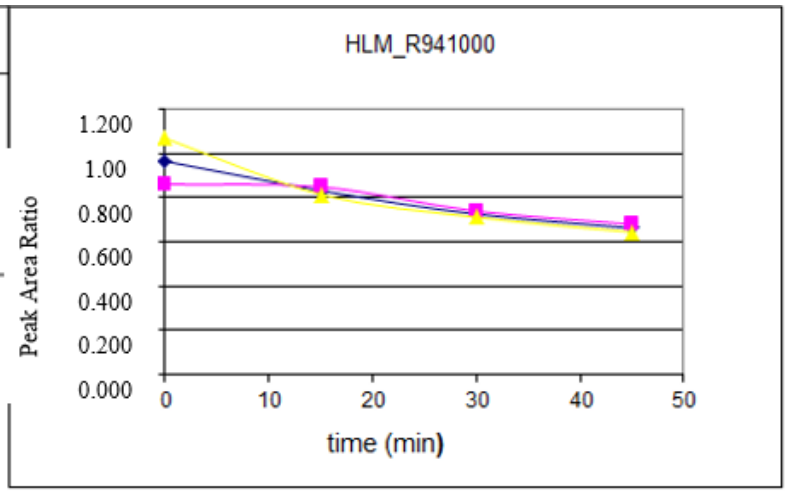

Figure 36. The stability of R941000 in HLM

Compound	RLM
R941000	>45 min
Midazolam	3.78
Propranolol	5.86

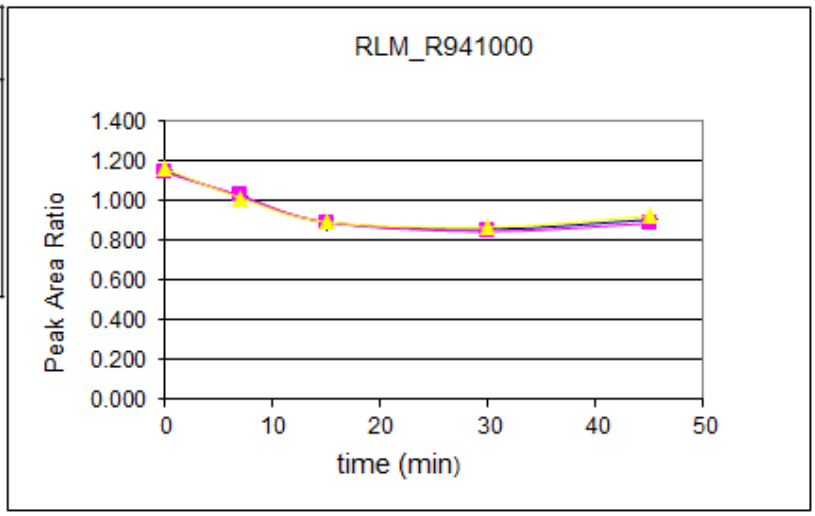

Figure 37. The stability of R941000 in RLM

In vitro data had thus far failed to significantly correlate with *in vivo* results; however, a modified supplemented microsome protocol was attempted. Several methods report improved UGT1A4 and UGT1A9 using 100 mM tris buffer pH 7.5-7.7 in human microsomes and expressed enzymes, while having no effect on other isoforms.[17] Both of these enzymes are capable of *N*-glucuronidation and may thus provide a more vigorous metabolism of R941000. While UGT1A4 and 1A9 are human UGTs (rodent homologs are inactive), it was hoped a change in buffer would result in improved R941000 glucuronidation. Results are shown in Figure 38 for the 2 h time points. Telmisartan acyl glucuronide formation had peak intensities of 10^6 cps, while no glucuronidation was observed for R941000.

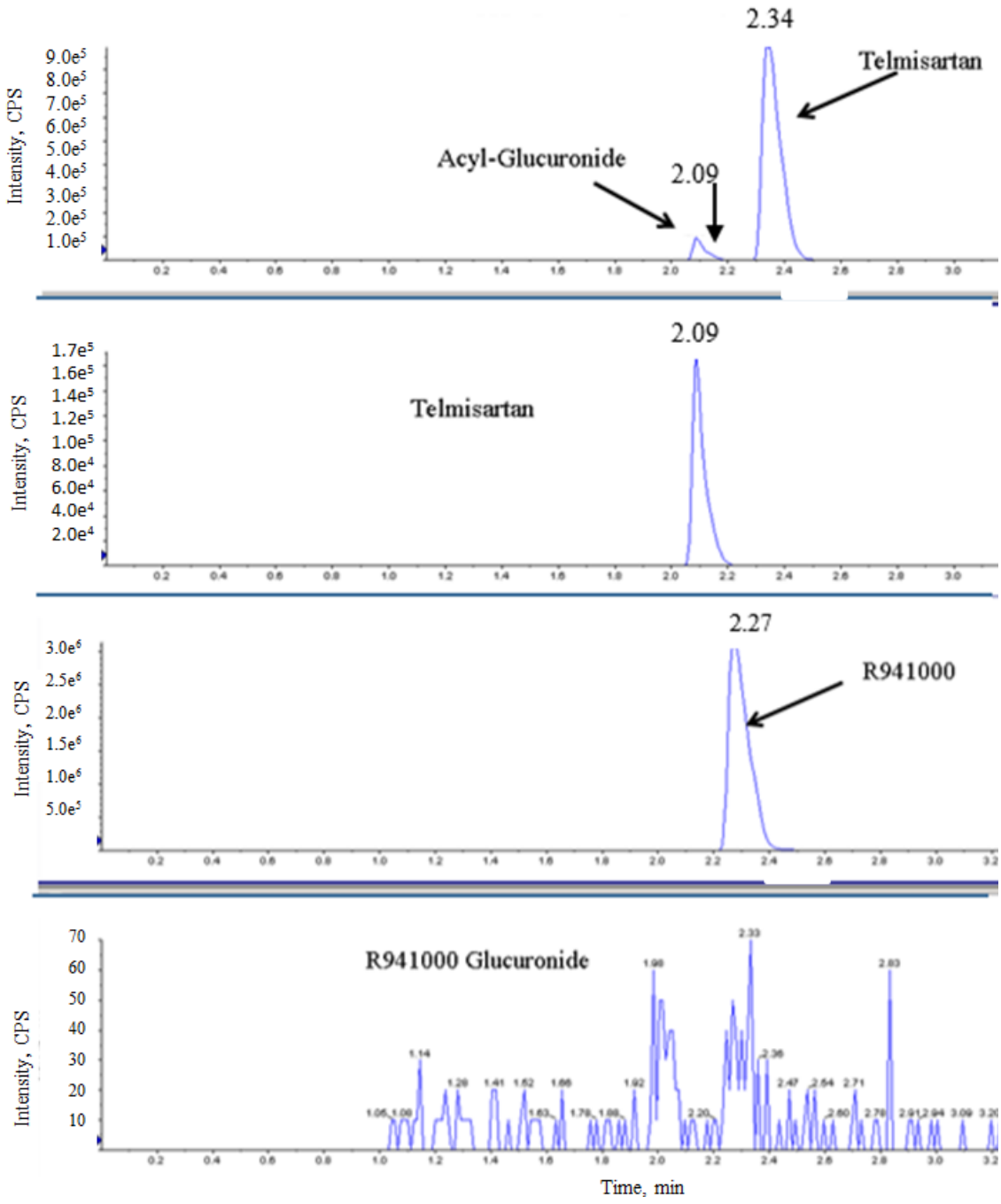

Figure 38. Incubation of R941000 in alamethicin treated RLM with tris-buffer. The two top chromatograms are the MRM transitions for telmisartan and its acyl glucuronide metabolite while the bottom two are of R941000 and its glucuronide metabolite.

4.0 Discussion

Recently, our lab demonstrated the feasibility of using a tetrazolone group as a bioisostere of a carboxylic acid for a number of compounds including telmisartan.[5] It was uncertain how replacement of this moiety with a tetrazolone would alter compound DMPK attributes. Thus, PK and metabolism studies were performed on the telmisartan-tetrazolone analog R941000 as an example of how disposition may be altered with this novel bioisostere.

Pharmacokinetics

R941000 total exposure levels and half-life were approximately 1.5 fold greater than telmisartan, while clearance was reduced about 1.5 fold. Volume of distribution for the two compounds was nearly identical, and bioavailability values were comparable at 65% and 59% for R941000 and telmisartan, respectively.

No significant hepatic first pass effect of R941000 was observed (HE <4%); however, telmisartan had an apparent HE of approximately 28%, and it was postulated that the lack of observed liver metabolism may partly explain the nearly threefold greater R941000 C_{max} values given the similar bioavailability of the compounds.

No R941000 or telmisartan was found in urine after 24 h, indicating biliary excretion into feces remains the predominant route of elimination; however, only 40-50% of either compound was recovered in feces, likely correlating to the fraction of compound not absorbed. Future studies with later time points are needed for a more definitive determination of excretion route.

Metabolism

In vivo metabolism studies with rat bile indicated differences in metabolism between the two compounds. Telmisartan is exclusively glucuronidated to an *O*-acyl glucuronide metabolite, while two major glucuronide metabolites were observed for R941000. Given the lack of glucuronidation occurring on the benzimidazole portion of telmisartan, it was postulated that glucuronidation of R941000 was occurring on the tetrazolone portion of the molecule, and that both an *N*- and *O*-glucuronide were being formed. Incubations with β glucuronidase in rat bile failed to eliminate the glucuronide peak preceding R941000 elution at 10.13 min, while the earlier eluting peak at 9.29 min disappeared, and an increase in peak intensity of R941000 was observed. Taken together, these results suggest a possible *N*-glucuronide at 10.13 min and *O*-glucuronide at 9.29 min. According to UV spectroscopy the alleged *N*-glucuronide and *O*-glucuronide made up 55% and 32% of all observed parent and metabolite species, respectively.

Glucuronidation of a tetrazolone as opposed to a carboxylic acid may have positive consequences, since carboxylic acids can form potentially toxic acyl glucuronides. Glucuronidated tetrazolone metabolites may be less prone to react with nucleophilic amino acid residues, which modify endogenous proteins, than their acyl glucuronide counterparts. As previously discussed, acyl glucuronides are capable of undergoing trans-acylation or acyl migration followed by ring opening and a subsequent Schiff-base reaction (see Figure 8) with electron rich amino acids.[10] Figures 39, 40, and 41 propose potential analogous acyl glucuronide reactivity pathways a tetrazolone glucuronide may undergo with nucleophilic amino acid residues.

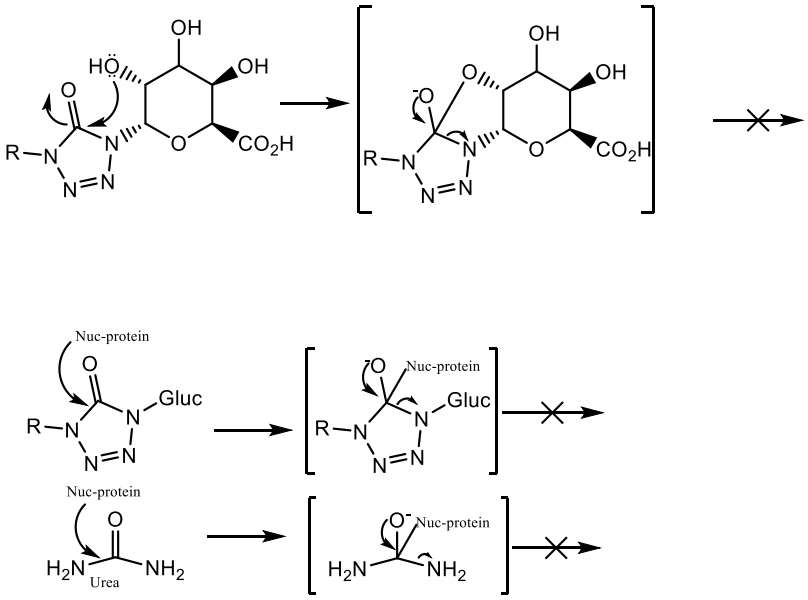

Figure 39. The potential of an *N*-glucuronidated tetrazolone to undergo tetrazolone migration is shown (top) along with its susceptibility to nucleophilic attack at the carbonyl (bottom).

Figure 39 depicts the likely inactivity of *N*-glucuronidated tetrazolones towards nucleophiles. Factors such as poor electrophilicity of the tetrazolone carbonyl (due to the donation of electrons from adjacent nitrogen atoms and the overall aromaticity of the tetrazolone) would make tetrazolones a poor candidate for nucleophilic attack. Moreover, the nitrogen glucuronide makes a poor leaving group, further reducing the likelihood of a direct nucleophilic attack on the tetrazolone carbon (depicted in the bottom of Figure 39 for a tetrazolone and urea as a "similar" carbonyl). For these same reasons, migration of the glucuronide around the tetrazolone would be unlikely as well; however, if the hydroxyl group on the 2 carbon of the glucuronide managed to attack the tetrazolone carbonyl, a five membered ring intermediate could form. The likelihood of this intermediate proceeding to another product is again improbable, since it would involve cleaving the nitrogen-carbon bond and forming an eight membered ring.

Figure 40 illustrates a possible mechanism for an *O*-tetrazolone glucuronide migration and Schiff-base reaction. The hydroxyl group on C2 may attack the tetrazolone carbonyl, forming a 5 member ring intermediate and allowing for a subsequent migration around the glucuronide. The glucuronide can alternate between closed and open forms, making it susceptible to a nucleophilic amino acid residue.

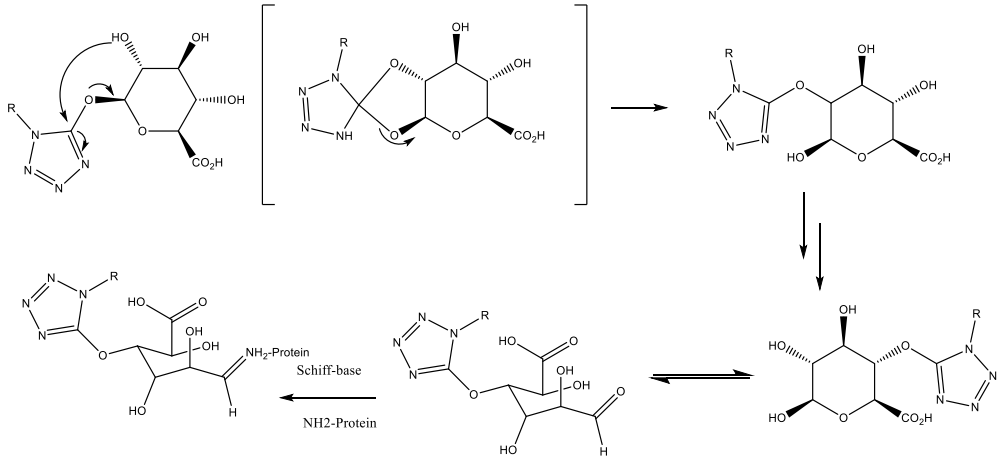

Figure 40. The potential toxicity of *O*-glucuronides through tetrazolone migration, ring opening, and glycation are shown.

There exists the possibility of a direct nucleophilic attack of *O*-glucuronide tetrazolones at the anomeric carbon of the glucuronide, the mechanism of which is shown in Figure 41. As can be seen, the anomeric carbon may be liable to nucleophilic amino acid residues; additionally, the tetrazolone would make a good leaving group, resulting in a glucuronidated protein. However, the only examples of trans-acylation occurring in literature happen on the carbonyl portion of the molecule, and it is uncertain at this point if the anomeric carbon would indeed be susceptible to nucleophilic attack.[10]

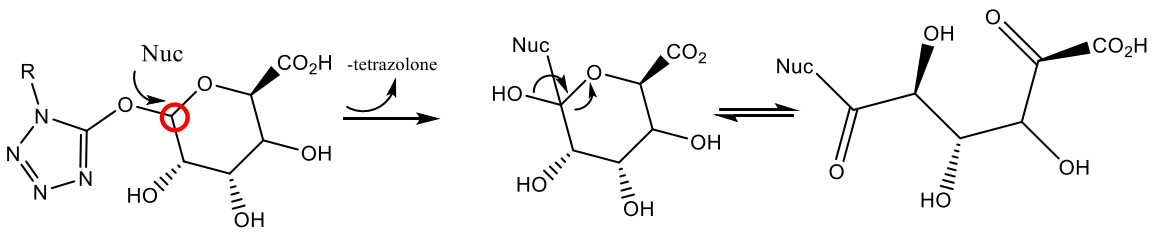

Figure 41. The potential reactivity of *O*-glucuronidated tetrazolone via glucuronidation is shown above.

While *N*-glucuronides may be unreactive to endogenous nucleophilic amino acids, the *O*-tetrazolone glucuronide could potentially possess a similar reactivity to that of an acyl glucuronide. Future studies incubating *O*- and *N*-glucuronide tetrazolones with nucleophiles mimicking *in vivo* conditions, such as thiols, may provide evidence confirming the liability (or lack thereof) of tetrazolones towards nucleophilic amino acid residues.

Various attempts to replicate *in vivo* metabolism in an *in vitro* assay failed to generate any significant amounts of tetrazolone glucuronides, though some oxidized metabolites were observed. Attempts at enhancing microsomal UGT with alamethicin yielded no R941000-glucuronide metabolites. With the lack of hepatic extraction observed, yet significant *in vivo* observation of glucuronide metabolites, it was thought glucuronidation may occur in the gut rather than the liver; however, incubation with alamethicin treated intestinal microsomes did not result in significant levels of glucuronidated metabolites, while those incubated with telmisartan did. Overall P450 contribution appeared minimal *in vitro* as well, with both telmisartan and R941000 showing microsomal stability > 45 min.

Conclusion

PK and metabolism analysis confirmed R941000 maintained similar to slightly improved PK profile in rat, while differing in metabolism with the formation of two major glucuronide metabolites. It is hypothesized that these glucuronides are an *N*-glucuronide and *O*-glucuronide. *In vitro* assays were unable to mimic *in vivo* results, and it is unclear where and what UGT isozyme is responsible for R941000 glucuronidation *in vivo*.

While only one compound and one preclinical species were assessed in this study, analysis of R941000 does provide a useful first step in demonstrating the feasibility of replacement of carboxylic acids with tetrazolones.

5.0 Future Studies

Currently, development of an *in vitro* assay mimicking *in vivo* results of R941000 glucuronidation is needed. Future studies using UGT expressed enzymes are planned to address this issue. UGT expressed enzymes may provide more robust UGT activity and will allow for identification of individual UGT isozymes responsible for glucuronidation if observed, thus potentially determining what enzyme(s) are responsible for the *N*- or *O*-glucuronide. Additionally, identification of the human recombinant UGT enzyme(s) may provide for a better understanding of potential human metabolism as well as potential drug-drug interactions. While an *N*- and *O*-glucuronide are the suspected metabolites, further characterization of these species is needed to definitively confirm their identity. Chemical synthesis of the proposed metabolites is being attempted and isolation of the

observed metabolites in sufficient quantities in bile for NMR analysis are currently underway.

Determining potential reactivity mechanisms of a compound or particular molecular moiety can be a long and arduous process, and one that sometimes may only become evident after a compound has been on the market for a number of years.[10-12] Indeed, much time, energy, and research have gone into developing the current hypothesis of acyl glucuronide toxicity.[10] However, there are a few assays that may be employed to test if tetrazolone glucuronides may be prone to interact with endogenous proteins in the same manner as acyl glucuronides. One method, as previously suggested, would be to incubate tetrazolone glucuronides with nucleophiles to assess their susceptibility to nucleophilic attack. A second method, developed by Sawamura and co-workers, correlates reactivity of acyl glucuronides with its stability in a buffer solution and its tendency towards acyl migration. The shorter the half-life, the more prone an acyl glucuronide is to migrate and react with electron rich amino acids.[12] In this paper, Sawamura tested several *O*-acyl glucuronide metabolites for compounds such as zomepirac (short half-life), diclofenac (intermediate half-life) and telmisartan (long half-life). Compounds forming acyl glucuronides with short half-lives were strongly correlated with toxicity and subsequent market withdrawal; those with intermediate half-lives were associated with warnings; those with good stability were considered "safe."[12] Synthesizing *O*- and *N*-glucuronide equivalents to compounds such as zomepirac, diclofenac, and telmisartan acyl glucuronides and testing their stability in buffer may provide an informative method of assessing potential reactivity and ranking of

tetrazolone glucuronides relative to each other and their acyl glucuronide counterparts.[12] Additionally, the stability of *N*-glucuronides may help confirm its inability for tetrazolone migration. Finally, animal studies comparing toxicity between tetrazolones and carboxylic compounds may provide a general yet informative study on the relative toxicity of this bioisostere to its carboxylic acid counter parts.

While the R941000 tetrazolone analog of telmisartan has thus far behaved as a carboxylic acid bioisostere, analysis of additional tetrazolone analogs is needed to better characterize this moiety as a carboxylic acid replacement since other tetrazolone analogs may have a different disposition and potency relative to their carboxylic acid counterparts. A larger set of examples would provide greater context into the range of disposition alterations caused by this bioisostere.

References

1. Ballatore, C.; Huryn, D., M.; Smith III, A. B. Carboxylic Acid (Bio)isosteres in Drug Design. *ChemMedChem.* **2013**, *8*, 385 – 396.

2. Williams, D. A.; Lemke, T. L.; *Foye's Principles of Medicinal Chemistry*, 5th ed.; Lippincott Williams & Wilkins: Massachusetts, 2002; chapter 2.

3. Papastavrou, N.; Chatzopoulou, M.; Kyriaki, P.; Nicolaou, L. 1-Hydroxypyrazole, as a Bioisostere of the Acetic Acid Moiety in a Series of Aldose Reductase Inhibitors. *Bmc.* **2013**, *21*, 4951–4957.

4. Graham, T. H., Shu, M.; Verras, A.; Chen, Q.; Garcia-Calvo, M.; Li, X.; Lisnock, J.; Tong; X.; Tung, E.; Wiltsie, J.; Hale, J. J.; Pinto, S. Pyrazoles as Non-Classical Bioisosteres in Prolycarboxypeptidase (PrCP) Inhibitors. *Bioorg. Med. Chem. Lett.* **2014**, *24*, 1657–1660.

5. Duncton, M.; Murray, R. *Unpublished Data.*

6. Gabrielsson, J.; Weiner, D. *Pharmacokinetic & Pharmacodynamic Data Analysis: Concepts and Applications*, 4th ed.; Swedish Pharmaceutical Society: Stockholm, Sweden, 2001; chapter 2.

7. Williams, D. A.; Lemke, T. L.; *Foye's Principles of Medicinal Chemistry,* 5th ed.; Lippincott Williams & Wilkins: Massachusetts, 2002; chapters 7-8.

8. Smith, D. A.; Bequmont, K.; Maurer, T. S.; Di, Li. Volume of Disposition in Drug Design. *J. Med. Chem.* **2015,** ahead of print.

9. Parkinson, A.; Ogivie, B. W.; Buckley, B. D.; Kazmi, F. K.; Czerwinski, M.; Parkinson, O. Chapter 6: Biotransformation of Xenobiotics, *Casarett & Doull's Toxicology, The Basic Science of Poisons.* 8th ed.; McGraw-Hill Education: Columbus, Ohio, 2013; 185 – 366.

10. Regan, S. L.; Maggs, J. L.; Hammond, T. G.; Lambert, C.; Williams, D. P.; Park, B. K. Acyl Glucuronides: The Good, The Bad and The Ugly. *Biopharm. Drug Dispos.* ***2010****, 31*, 367–395.

11. Jinno, N.; Ohashi, S.; Tagashira, M.; Kohira, T.; Yamada, S. A Simple Method to Evaluate Reactivity of Acylglucuronides Optimized for Early Stage Drug Discovery. *Bio. Pharm Bull.* ***2013****, 36* 1509–1513.

12. Sawamura, R.; Okaudaira, N.; Watanabe, K.; Murai, T.; Kobayshi, Y.; Tachibana, M.; Ohnuki, T.; Masuda, K.; Honma, H.; Kurihara, A.; Okazaki, O. Predictability of Idiosyncratic Drug Toxicity Risk for Carboxylic Acid-Containing Drugs Based on the Chemical Stability of Acyl Glucuronide. *DMD.* **2010**, *38*, 1857–1864.

13. Fitch, B.; Miao, S.; *BAAC Workshop: Drug metabolism & Metabolite Identification.* March 05, 2013, Foster City, CA USA.

14. Caldwell, G. W.; Yan. Z.; 2nd ed. *Optimization In Drug Discovery In vitro Methods,* 2nd ed.; Humana Press: Springer, New York, 2014; Chapters 6-7.

15. Fisher, M. B., Campanale, K.; Ackermann, B. L.; Vandenbranden, M.; Wrighton, S. A. *In vitro* Glucuronidation Using Human Liver Microsomes and the Pore-forming Peptide Alamethicin. *DMD.* **2000**, *28*, 560–566.

16. Oleson, L.; Court, M. H. Effects of β-Glucuronidase Inhibitor Saccharolactone on Glucuronidation by Human tissues and recombinant UDP-Glucuronsyltransferases (UGTs). *J. Pharm Pharmacol.* **2008**, *60*, 1175–1182.

17. Walsky, R. L.; Bauman, J. N., Bourcier, K.; Giddens, G.; Lapham, K.; Negahban, A.; Ryder, T. F.; Obach, R. S.; Hyland, R.; Goosen, T. C. Optimized Assays for Human UDP-Glucuronsyltransferase (UGT) Activities: Altered Alamethicin Concentration and Utility to Screen for UGT Inhibitors. *DMD.* **2012**, *40 5*, 1051–1065.

18. Giuliano, C.; Jairaj, M.; Zafiu, C. M.; Laufer, R. Direct Determination of Unbound Intrinsic Drug Clearance in the Microsomal Stability Assay. *DMD,* **2005**, *33*, 1319–1324.

19. Caldwell, G. W.; Yan. Z.; 2nd ed. *Optimization In Drug Discovery In vitro Methods,* 2nd ed.; Humana Press: Springer, New York, 2014; Chapter 25.

20. Henion, J.; CCO-PBSS San Francisco Bay Area Workshop: *Advanced LC/MS Practices.* Jan. 2013, Foster City, CA USA.

21. Skoog, A. D.; Hooler, F. J.; Nieman, T. A. *Principles of Instrument Analysis,* 5th ed. Saunders College Publishing: Florida, 1998; Chapters 26-28.

22. Skoog, A. D.; Hooler, F. J.; Nieman, T. A. *Principles of Instrument Analysis*, 5th ed.; Saunders College Publishing: Florida, 1998; Chapter 20.

23. www.chem.agilent.com/Library/eseminars/Public/Mass Accuracy and Mass Resolution - October 2011.pdf

24. Brenton, G. A.; Godfrey, R. A.; Accurate Mass Measurement: Terminology and Treatment of Data. *J. Am Soc Mass Spectrom*, **2010**, *21*, 1821–1835.

25. Wienen, W.; Entzeroth, M.; vanMeel, J. C. A.; Stangier, J.; Busch, U.; Ebner, T.; Schmid, J.; Lehmann, H.; Kandace, M.; Kempthorne-Rawson, J.; Gladigau, V.; Hauel, N. H. A Review on Telmisartan: A Novel, Long-Acting Angiotensin II-Receptor Antagonist. *Cardiovascular Drug Reviews*. **2000,** *18* (2), 127 – 154.

26. Takashima, T.; Hashizume, Y.; Katayama, Y.; Murai, M.; Wada, Y.; Maeda, K.; Sugiyama, Y.; Watanabe, Y. The Involvement of Organic Anion Transporting Polypeptide in the Hepatic Uptake of Telmisartan in Rats: PET Studies with [^{11}C] Telmisartan. *Mol. Pharmaceutics*. **2011**, (8I), 1789 – 1798.

27. HAO, K.; Chen, Y-C.; CAO, Y. G.; YU, D.; LIU, X. Q.; WANG, G. J. Pharmacokinetic-Pharmacodynamic Modeling of Telmisartan Using an Indirect Response Model in Spontaneously Hypertensive Rats. *Acta Pharmacol Sin*. **2007**, *28 (5)*, 738 – 743.

28. www.xenotech.com/flyers/hepatocytes/cryopreserved-hepatocyte-thawing-protocol.pdf

29. Zenser, T. V.; Lakshmi, V. M., Davis, B. B.; Human and *Escherichia coli β*-Glucuronidase Hydrolysis of Glucuronide Conjugates of Benxide and 4-aminobiphenyl, and Their Hydroxy Metabolites. *DMD*. **1999**, *27*, 1064–1067.

30. Frandsen, H. L.; *Food and Toxicology*. **2007**, *45*, 863–870.